Wetting: statics and dynamics

P. G. de Gennes

Collège de France, Physique de la Matière Condensée, 11 Place Marcelin-Berthelot, 75231 Paris Cedex 05, France

The wetting of solids by liquids is connected to physical chemistry (wettability), to statistical physics (pinning of the contact line, wetting transitions, etc.), to long-range forces (van der Waals, double layers), and to fluid dynamics. The present review represents an attempt towards a unified picture with special emphasis on certain features of "dry spreading": (a) the final state of a spreading droplet need not be a monomolecular film; (b) the spreading drop is surrounded by a precursor film, where most of the available free energy is spent; and (c) polymer melts may slip on the solid and belong to a separate dynamical class, conceptually related to the spreading of superfluids.

CONTENTS

I. INTRODUCTION

Many practical processes require the spreading of a liquid on a solid. The liquid may be a paint, a lubricant, an ink, or a dye. The solid may either show a simple surface or be finely divided (suspensions, porous media, fibers). Water, for instance, may be sucked into a porous soil, because it tends to wet the solid components of the soil. Tertiary oil recuperation also involves the penetration of water into the channels of a porous rock, which were originally filled mainly by oil. The "flotation" of ores is based on selective wetting properties for the ore particles.

In spite of their importance, these processes are still poorly understood.

(1) All interfacial effects are very sensitive to contaminants and to physical modifications of the surface (e.g., steps, dislocations, if we are dealing with a crystalline solid); this may explain why certain basic experiments (e.g., spreading a single small droplet on a flat solid surface) have been fully carried out only recently.

(2) The solid/liquid interfaces are much harder to probe than their solid/vacuum counterpart; essentially all experiments making use of electron beams become inapplicable when a fluid is present. A few sensitive techniques may still be applied specifically to the interface (fluorescence, EPR, etc.), but they are often restricted to very specific examples. Similar limitations occur with the electrochemical data.

(3) On the theoretical side, 180 years after the pioneering work of Young and Laplace, a number of basic capillary problems are just beginning to be solved.

(a) The physicochemical parameters controlling the *thermodynamic wettability* of solid surfaces were clarified through the long, careful efforts of Zisman (1964) and others (Fowkes, 1964; Padday, 1978), but the deviations from thermodynamic equilibrium are just beginning to be understood. Here I shall insist particularly on two such deviations—the hysteresis of contact angles, due to the pinning of the contact line on localized defects, and the regimes of "dry spreading," where the final state of a spreading droplet is not necessarily a monomolecular layer, but may be a film of greater thickness. These relatively novel aspects are explained in Sec. II.

(b) The transition from "*complete wetting*" to "*partial wetting*" (defined in Fig. 1 below), first predicted in 1977 (Cahn, 1977; Ebner and Saam, 1977), has become an active field of research and dispute (Sec. III).

(c) The *dynamics* of spreading is delicate: a pioneering paper (Huh and Scriven, 1971) suggested a singularity in the dissipation, which provoked many discussions. Recently, a useful distinction has appeared between simple fluids, in which the liquid spreads by a rolling motion (Dussan and Davis, 1974), and polymer melts, which often tend to slip on a solid surface (Brochard and de Gennes, 1984). These two regimes (and the corresponding removal of singularities) are presented in Sec. IV.

Our discussion does not include the *local* structure of the interfaces—the arrangement of the atoms, or molecules, at the 3-Å scale near a boundary. For fluid/fluid interfaces, this aspect is, in fact, well reviewed in a recent book (Rowlinson and Widom, 1982). For solid/fluid interfaces our knowledge is still rather limited. In the present paper, the emphasis will be on behavior at somewhat larger scales (say 30 to 300 Å), where long-range forces (van der Waals, electrostatic, etc.) become essential, control many practical features, and give rather universal properties.

II. CONTACT ANGLES

A. Thermodynamic equilibrium

1. Angles and energies: the Young condition

When a small liquid droplet is put in contact with a flat solid surface, two distinct equilibrium regimes may be found: partial wetting [Figs. 1(a) and 1(b)] with a finite contact angle θ_e, or complete wetting ($\theta_e=0$) [Fig. 1(c)].[1] In cases of partial wetting, the wetted portion of the surface is delimited by a certain *contact line* $\mathscr{L}$ (which, for our droplets, is a circle).

The situation near the contact line is represented more precisely in Fig. 2. Here we are dealing with a macroscopic wedge, and the line $\mathscr{L}$ is normal to the plane of the figure. Three phases are in contact at the line: the solid S, the liquid L, and the corresponding *equilibrium vapor* V. Each interface has a certain free energy per unit area γ_{SL}, γ_{SV}, and γ_{LV} (the latter, for simplicity, will simply be called γ).

These parameters describe adequately the energy content of the interfaces in the far field (far from $\mathscr{L}$). In the vicinity of $\mathscr{L}$, the structure is much more complex and depends on a detailed knowledge of the system (examples of the complications that may occur are shown in Fig. 3). There is a "core region" around the nominal position of $\mathscr{L}$, where the complications occur. It is possible, however, to relate θ_e to the far-field energies γ_{ij} *without any knowledge of the core.* This was one of the (many) discoveries of the British scientist Thomas Young (1773–1829).

The basic idea is to write that, in equilibrium, the energy must be stationary with respect to any shift (dx) of the line position. In such a shift, (a) the bulk energies are unaffected (since the pressure is the same in the liquid and in the vapor); (b) the core energy is unaffected—the core is simply translated; and (c) the areas of the far-field interfaces (for a unit length of line) are increased, respectively, by dx (for S/V), $-dx$ (for S/L), and $-\cos\theta_e dx$ (for L/V). Hence the condition

$$\gamma_{SV}-\gamma_{SL}-\gamma\cos\theta_e=0\ . \tag{2.1}$$

[1]The subscript (e) in θ_e refers to an *equilibrium* property.

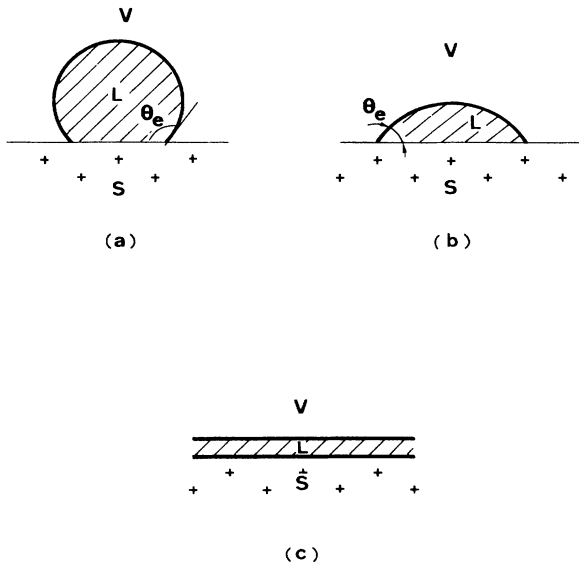

FIG. 1. A small droplet in equilibrium over a horizontal surface: (a) and (b) correspond to partial wetting, the trend towards wetting being stronger in (b) than in (a). (c) corresponds to complete wetting ($\theta_e = 0$).

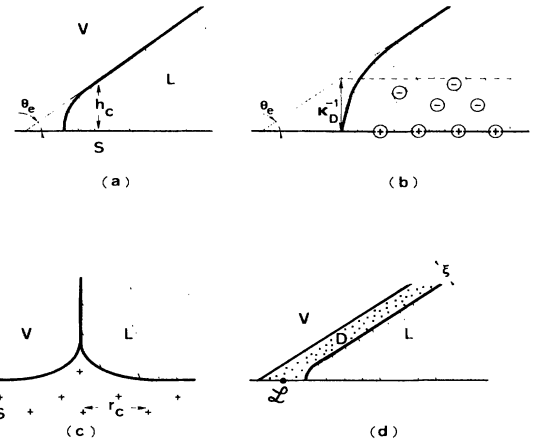

FIG. 3. Various types of core structures for the triple line. (a) Effect of attractive van der Waals forces. For $\theta_e \ll 1$, the profile is hyperbolic and the height h_c of the perturbed region is of order a/θ_e (where a is an atomic length). (b) A charged solid surface wetted by salty water (screening length κ_D^{-1}). (c) Effect of the finite deformability of the solid. The width r_c of the deformed region is $r_c \sim \gamma/E$ (γ, surface tension of the liquid; E, Young's modulus of the solid). For simplicity the special case $\theta_e = \pi/2$ has been drawn. (d) In the vicinity of a liquid/vapor critical point, the L/V interface becomes diffuse (thickness ξ) and the triple line has a core of radius $r_c \sim \xi$.

Equation (2.1) shows that the angle θ_e is entirely defined in terms of thermodynamic parameters: measurements on θ_e give us certain information on the interfacial energies. Usually, we know $\gamma_{LV} \equiv \gamma$ by separate measurements. Thus we are left with two unknowns (γ_{SL}, γ_{SV}) and only one datum (θ_e). But it is only the *difference* $\gamma_{SV} - \gamma_{SL}$ which is relevant for experiments involving the liquid.

2. Spatial scales for the definition of a contact angle

Equation (2.1) was derived for a wedge (planar interfaces in the far field). For many practical applications (such as the droplets of Fig. 1), some weak curvatures are superimposed.

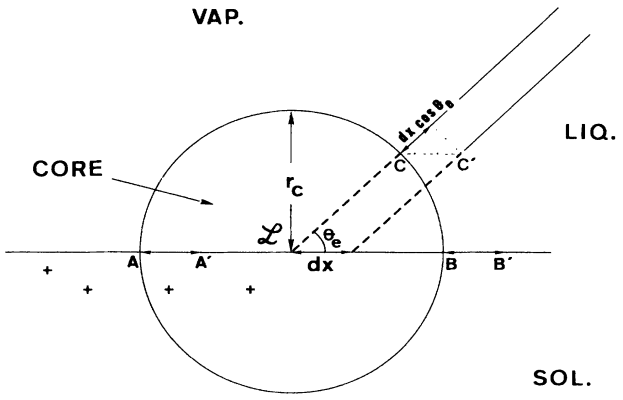

FIG. 2. Translation of a liquid wedge (triple line $\mathscr{L}$) by an amount dx. The energy is unchanged in this process, and this leads to the Young equation (2.1).

(a) The liquid/vapor interface may have a total curvature $C = R_1^{-1} + R_2^{-1}$, and this is associated with a certain pressure difference between liquid and vapor:[2]

$$p_L - p_V = \gamma C \ . \tag{2.2}$$

The angle θ_e is still well defined in this case, provided that the radii of curvature (R_1, R_2) *are much larger than the size (r_C) of the core region.*

(b) The line $\mathscr{L}$ itself may be curved, and, in this case, a displacement of the line modifies the core energies. Again, this leads to measurable effects only when the radius of curvature of the line is not too large, when compared to the core size r_C [see, for instance, Platikhanov *et al.* (1980)]. In many practical examples $r_C < 100$ Å. Thus, for most macroscopic experiments, where the droplets or the capillaries have sizes $R \sim 1$ mm, all curvature corrections are negligible. A measurement of θ_e at a distance r from the line, where

$$r_C \ll r \ll R \ ,$$

should give a well-defined θ_e, independent of r.

[2]Equation (2.2) is also due to Young (1804) and was rediscovered independently one year later by Laplace.

3. Practical determinations of θ_e

The angle θ_e can be obtained (a) from a direct photograph, (b) through the reflection (or deflection) of rays by the liquid prism of Fig. 2, (c) by interferential techniques (Callaghan *et al.*, 1983), especially for small θ_e, (d) from the rise of a liquid column in a fine capillary (Fig. 4); for a general discussion of the various capillary effects, see the classical book by Bouasse (1924) and the recent tutorial article of Guyon *et al.* (1982).

In actual experiments the main difficulty is to avoid a certain *pinning of the triple line* $\mathscr{L}$ on defects of the solid surface. This pinning leads to a hysteresis of the contact angles, which can very seriously obscure the determination of θ_e. Clearly, to avoid pinning one requires solid surfaces that are smooth and chemically homogeneous, but the question is, what level of smoothness do we require to reduce the uncertainty in θ_e below a prescribed limit $\Delta\theta$? A partial answer to this question is given in Sec. II.C.

4. Special features of complete wetting

Equation (2.1) gives $\cos\theta_e$ as a function of interfacial energies. The special case

$$\gamma = \gamma_{SV} - \gamma_{SL}$$

leads to $\cos\theta_e = 1$ or $\theta_e = 0$ (complete wetting). At first sight, this situation appears rather exceptional. In fact, it is not, because $\gamma_{SL} + \gamma$ can never be larger than γ_{SV} (in thermodynamic equilibrium). If it were larger, this would imply that the free energy of a solid/vapor interface (γ_{SV}) could be lowered by intercalating a liquid film of macroscopic thickness (energy $\gamma_{SL} + \gamma$). The equilibrium solid/vapor interface then automatically comprises such a film, and the true γ_{SV} is identical to $\gamma_{SL} + \gamma$, i.e., we have complete wetting in this regime.

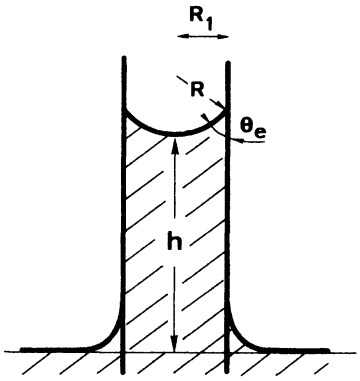

FIG. 4. Capillary rise: in a thin capillary the meniscus is a spherical cap of radius $R = R_1/\cos\theta_e$. The Young-Laplace capillary pressure $2\gamma/R$ is balanced by the hydrostatic component $\rho g h$ (ρ, density difference between liquid and vapor, g, gravitational constant). Thus a measurement of h gives θ_e.

On the other hand, if we deal with nonequilibrium situations, we may have a solid/vapor interfacial energy γ_{SO} that is larger than $\gamma_{SL} + \gamma$. The difference

$$S = \gamma_{SO} - \gamma_{SL} - \gamma \tag{2.3}$$

is called the spreading coefficient. Physically, γ_{SO} is associated with a "dry" solid surface, while γ_{SV} is associated with a "moist" surface. For some systems the difference is enormous. With water on metallic oxides, $\gamma_{SO} - \gamma_{SV} \sim 300$ ergs/cm^2; with organic liquids on oxides, $\gamma_{SO} - \gamma_{SV} \sim 60$ ergs/cm^2. On the other hand, with organic liquids on molecular solids, the difference (as seen via contact angles) is perceptible only when the liquid is very light and volatile. For instance, with normal alcanes on a Teflon surface, the angles θ_0 (on dry Teflon) and θ_e (in equilibrium with the vapor) are found to differ only when the carbon number n of the alcane is ≤ 5 (Zisman, 1964).

The importance of the spreading coefficient (2.3) for practical purposes was first recognized by Cooper and Nuttal (1915) in connection with the spraying of insecticides on leaves. Large positive S favors the spreading of a liquid.

There remains, however, a fundamental ambiguity in cases where the experimentalist observes complete spreading on macroscopic scales: he cannot tell whether $S = 0$ or $S > 0$. For the "moist" case, we know that $\theta_e = 0$ (or that the corresponding $S_{\text{moist}} \equiv 0$) because the system "locks in" at this value, as explained at the beginning of this section. But for the "dry" case there is no "lock-in" process, and we expect that complete spreading will usually be associated with a positive S.

How large is S? We shall see in Sec. II.D that the answer may sometimes be obtained by probing the thickness of the ultimate wetting film achieved in spreading: the smaller the S, the larger the equilibrium thickness, in qualitative agreement with the trend noticed by Cooper and Nuttal.

B. Wettability

Our aim in this section is to understand qualitatively how the contact angle θ_e depends on the chemical constitution of both the solid S and the liquid L. The basic reference here is still the review by Zisman (1964).

1. High-energy and low-energy surfaces

Let us discuss the solid first. From studies on the bulk cohesive energy we know that there are two main types of solids, (a) hard solids (covalent, ionic, or metallic), and (b) weak molecular crystals (bound by van der Waals forces, or in some special cases, by hydrogen bonds). A similar classification is found from the solid/vacuum surface energies (Fox and Zisman, 1950). Hard solids have "high-energy surfaces" ($\gamma_{SO} \sim 500$ to 5000 ergs/cm^2), while molecular solids (and also molecular liquids) have "low-energy surfaces" ($\gamma_{SO} \sim 50$ ergs/cm^2).

2. Standard behavior of high-energy surfaces

Most molecular liquids achieve complete wetting ($S \geq 0$) with high-energy surfaces. Let us try to understand this in simple terms, assuming that hard bonds control γ_{SO}, while van der Waals interactions control the liquid/solid energies (no chemical binding between liquid and solid). This amounts to writing for the solid/liquid energy

$$\gamma_{SL} = \gamma_{SO} + \gamma - V_{SL} \quad (V_{SL} > 0) \, . \tag{2.4}$$

Here the term $-V_{SL}$ describes the attractive van der Waals (VW) interactions between solid and liquid near the surface. Equation (2.4) can be understood if we progressively bring into contact the regions S and L; when they are well separated (by an empty slab), the energy is $\gamma_{SO} + \gamma$; when we establish contact, we recover the energy $-V_{SL}$.

Very similarly, by bringing into contact two *liquid* portions, we start with an energy 2γ, and end up with zero interfacial energy,

$$0 = 2\gamma - V_{LL} \quad (V_{LL} > 0) \, , \tag{2.5}$$

where $-V_{LL}$ represents the LL attractions. Using Eqs. (2.4) and (2.5), we find that the spreading parameter S, defined in Eq. (2.3), is equal to

$$S = -2\gamma + V_{SL} = V_{SL} - V_{LL} \, ,$$

and the condition of complete wetting ($S > 0$) corresponds to

$$V_{SL} > V_{LL} \, . \tag{2.6}$$

It is also possible to translate (2.6) in terms of the dielectric polarizabilities α_S (α_L) for the solid (liquid). To a first approximation the VW couplings between two species (i) and (j) are simply proportional to the product of the corresponding polarizabilities

$$V_{ij} = k\alpha_i\alpha_j \, , \tag{2.7}$$

where k is (roughly) independent of (i) and (j). Then the condition (2.6) reduces to

$$\alpha_S > \alpha_L \, . \tag{2.8}$$

Thus high-energy surfaces are wetted by molecular liquids, not because γ_{SO} is high, but rather because the underlying solid usually has a polarizability α_S much higher than the polarizability of the liquid. Of course, these considerations are very rough (the frequency dependence of the α's should be taken into account), but they still provide us with some guidance.

3. Low-energy surfaces and critical surface tensions

Low-energy surfaces can give rise to partial or to complete wetting, depending on the liquid chosen. In a complex situation like this, it is natural to choose a series of homologous liquids (for instance, the n-alcanes) and to study how they wet a given solid.

In some cases we find complete wetting for the whole series. This occurs, for instance, for liquid alcanes against solid polyethylene. But in other cases we find a finite contact angle θ_e, varying within the homologous series. A useful way of representing these results is to plot $\cos\theta_e$ versus the surface tension γ of the liquid. (An example is shown in Fig. 5.) Although, in many cases, we never reach $\cos\theta_e = 1$, i.e., we never reach complete wetting, we can extrapolate the plot down to a value $\gamma = \gamma_C$, which would correspond to $\cos\theta_e = 1$. The details of the extrapolation produced differ from author to author (in the pioneering work of Zisman a linear extrapolation was used), but this is not essential.

In general, we would expect γ_C to depend on the solid S, but to depend also on the liquid series L. However, when dealing with simple molecular liquids (where van der Waals forces are dominant), Zisman observed that γ_C is essentially independent of the nature of the liquid, and is a characteristic of the solid alone. Typical values are listed below:

	ergs/cm^2
Nylon	46
P. Vinyl chloride	39
P. Ethylene	31
PVF_2	28
PVF_4	18

If we want to find a molecular liquid that wets completely a given low-energy surface, we must choose a liquid of surface tension $\gamma < \gamma_C$. Thus γ_C may be called a "critical surface tension" and is clearly the essential parameter for many practical applications.

Can we relate γ_C to some simple physical parameters of the solid? This has been attempted by various authors

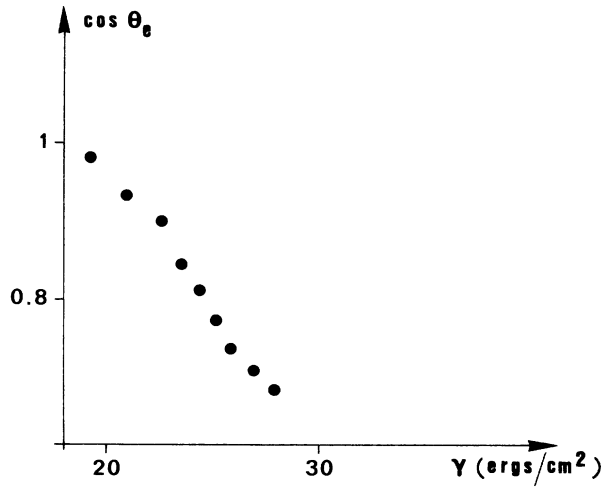

FIG. 5. A typical Zisman plot (cosine of equilibrium angle θ_e vs surface tension) for a polytetrafluoroethylene (Teflon) surface in contact with liquid n-alkanes (after Fox and Zisman, 1950). The critical surface tension γ_c for this system is ~ 18 ergs/cm^2.

(Girifalco and Good, 1957; Fowkes, 1962; Good, 1964). In the present review, we shall present only a naive argument, following the simple "van der Waals model" of Eqs. (2.4)—(2.7) and always assuming that the polarizability γ_V of the vapor is negligible. This amounts to writing

$$\begin{aligned}\cos\theta_e &= \frac{\gamma_{SV}-\gamma_{SL}}{\gamma} \\ &\cong \frac{\gamma_{SO}-\gamma_{SL}}{\gamma} \\ &\cong \frac{V_{SL}-\gamma}{\gamma} \\ &= \frac{2\alpha_S}{\alpha_L}-1 \ . \end{aligned} \tag{2.9}$$

When we compare different chemicals within the same homologous series, we vary α_L. For instance, with alcanes, the polarizability of the terminal (CH_3) groups is higher than the polarizability of the $-CH_2-$ groups: shorter alcanes have larger α_L values. The value of α_L at which $\cos\theta_e$ extrapolates to 1 is

$$\alpha_{LC}=\alpha_S \ . \tag{2.10}$$

If we prefer to work in terms of surface tensions $\gamma=\frac{1}{2}V_{LL}=\frac{1}{2}k\alpha_L^2$, we may write Eq. (2.9) in the form

$$\cos\theta_e = 2\left[\frac{\gamma_C}{\gamma}\right]^{1/2}-1 \ , \tag{2.11}$$

$$\gamma_C=\tfrac{1}{2}k\alpha_S^2 \ . \tag{2.12}$$

Equation (2.12) does show that γ_C depends only on the properties of the solid and is an increasing function of its polarizability. Numerically, Eq. (2.12) is not good, and various lines of improvement have been pursued.

(a) In practice many forces contribute to the solid/liquid interactions—dipolar, hydrogen bonds, etc. Thus one adds more terms in the decomposition (2.4), each force giving its contribution to V_{SL} and to V_{LL} (see, for instance, Good, 1964). In such a case γ_C may depend slightly on the nature of the liquids chosen to define it.

(b) Even when VW forces only are present, the simple expression (2.7) of the interaction in terms of some average polarizabilities is too primitive. More precise theories incorporate the frequency dependence of the polarizabilities, following the lines of the Lifshitz calculation of VW forces (Owens *et al.*, 1978). We shall not insist on these points, but mention that there exists (at least) a third group of corrections.

(c) The density distribution and the pair correlations in the liquid are modified near the solid surface, and these modifications may be quite different from what they are at the free surface of the liquid. For instance, recent work by Israelashvili (1982) and others shows that the forces between two closely spaced (20 Å) solid surfaces, through a liquid, are often oscillatory in sign, suggesting a one-particle density function in the liquid, which oscillates as a function of the distance to the solid. Computer work on these structures has begun (see, for instance, Snook and Van Megen, 1979,1980), but some more time will be required before we extract from it some really general rules and trends.

Let us now return to the practical aspects, and comment upon the values of γ_C that have been listed above.

(a) The system of high γ_C (nylons, PVC) are those most wettable by organic liquids. They carry rather strong permanent dipoles.

(b) Among systems that are controlled by VW interactions, we note that CF_2 groups are less wettable ($\leftrightarrow$ less polarizable) than CH_2 groups. In practice, many protective coatings (antistain, waterproofing, etc.) are based on fluorinated systems.

(c) It is possible to study specifically the wetting properties of terminal groups CF_3- or CH_3- by depositing a surfactant monolayer on a polar solid surface (Fig. 6). For CH_3 groups $\gamma_L=24$ ergs/cm^2, and for CF_3, γ_C is amazingly small (~ 6 ergs/cm^2). For more details on all these fascinating questions, we again refer the reader to the beautiful review by Zisman (1964).

C. Contact angle hysteresis

1. Experiments

The determination of the thermodynamic contact angle requires very clean experimental conditions. In many practical situations, one finds that the triple line $\mathscr{L}$ is pinned, and immobile, not only for $\theta=\theta_e$ but whenever θ lies within a finite interval around θ_e,

$$\theta_r<\theta<\theta_a \ . \tag{2.13}$$

The angle θ_a (advancing angle) is measured when the solid/liquid contact area increases, while θ_r (receding an-

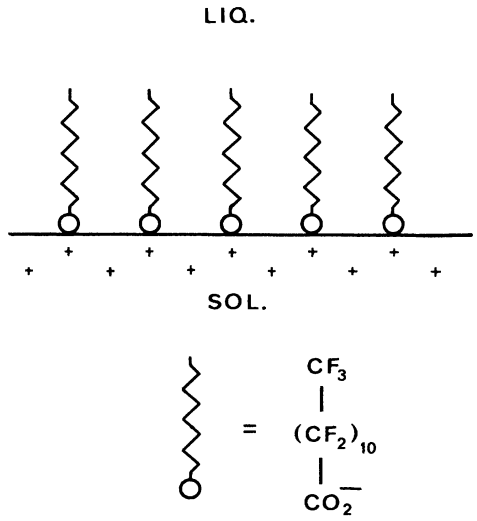

FIG. 6. Idealized structure of a surfactant monolayer attached to a polar solid. The particular example chosen provides one of the least wettable surfaces ever found.

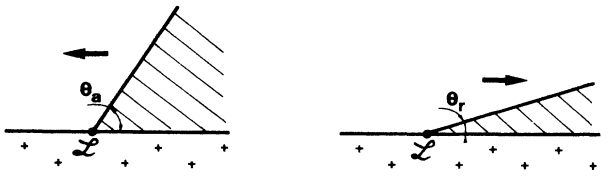

FIG. 7. Definition of the advancing (θ_a) and receding (θ_r) angles for a liquid on a nonideal solid surface.

gle) is measured when the contact area shrinks (Fig. 7). The interval $\theta_a - \theta_r$ may be 10° or more for surfaces that have not been specially prepared.

What is the source of this hysteresis? Three major causes have been invoked.

(a) *Surface roughness.* Early observations by Trillat and Fritz (1937) showed that the triple line $\mathscr{L}$ was easily trapped when parallel to a system of grooves. Among the more recent experiments, those by Dettre and Johnson (1964) deserve special mention because they were performed with a series of solid surfaces of increasing roughness. A typical set of data is shown in Fig. 8. It exhibits a remarkable, nonmonotonous variation of θ_r with the degree of roughness, to which we shall return later. Further systematic studies were carried out by Mason (1978).

(b) *Chemical contaminations,* or inhomogeneities, in the solid surface may also play an important role. Some of the experiments of Dettre and Johnson (1964) were made with glass beads immersed in paraffin wax, and the differences in wettability between glass and paraffin may have contributed to the hysteresis. But systematic studies of purely chemical effects at a smooth surface are still lacking.

(c) *Solutes* in the liquid (surfactants, polymers, etc.) may deposit a film on the solid surface, and the presence or absence of the film can, in some cases, lead to hysteretic effects. In many cases the film, once formed, is stuck on the solid surface. See, for instance, Chappuis (1984).

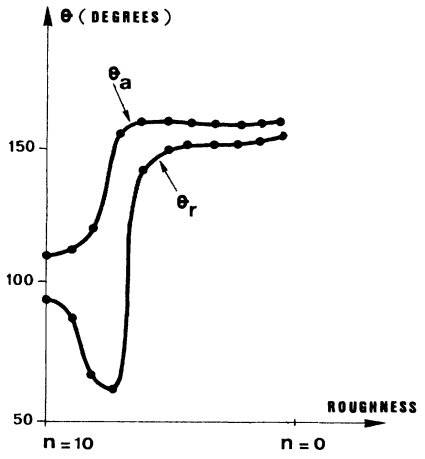

FIG. 8. Advancing and receding angles for water on fluorocarbon wax: a rough surface is obtained by spraying the wax. It is then made smoother by heating in an oven. The numbers n on the horizontal scale (0,1.0,10) refer to the number of successive heat treatments. Notice the abrupt jump of θ_r between $n=6$ and $n=7$ (after Dettre and Johnson, 1964).

2. Models with parallel grooves

Early discussions on the effects of surface roughness were restricted to *periodic* surfaces—for instance, with a parallel set of grooves (Johnson and Dettre, 1964; Mason, 1978; Cox, 1983). These systems have some reality—a classical example is a phonograph record (Oliver *et al.*, 1977).

When the triple line $\mathscr{L}$ is parallel to the grooves, it may have a number of pinned positions (described in Fig. 9), and it is possible to compute numerically the magnitude of the energy barriers between two such positions. Some aspects of these calculations are very artificial (the energy barriers are proportional to the total length of line

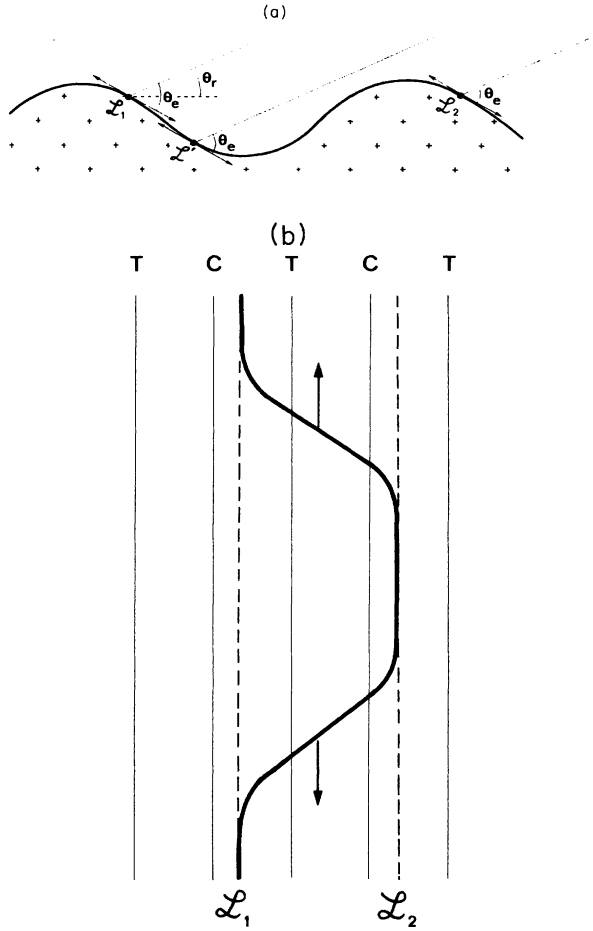

FIG. 9. (a) Equilibrium positions of a contact line $\mathscr{L}$ (normal to the sheet) on a system of grooves. $\mathscr{L}_1$, $\mathscr{L}_2$, are locally stable, while $\mathscr{L}'$ is unstable. θ_e is the thermodynamic contact angle. θ_r is the macroscopic angle. (b) The creep process for a contact line $\mathscr{L}$ moving from position $\mathscr{L}_1$ to position $\mathscr{L}_2$. C stands for "crest" and T for "trough."

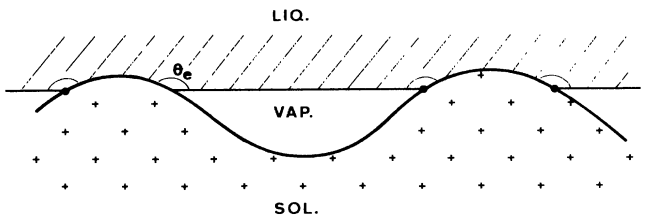

FIG. 10. A "composite" structure, with vapor bubbles trapped between liquid and solid, when the solid has deep, parallel grooves.

involved), but some aspects are instructive. For instance, when the grooves are rather deep, it may happen that vapor bubbles remain locked in the troughs and are covered by the liquid (Fig. 10). The resulting "composite structures" are then predicted to display much smaller barriers. The minimum of θ_r are a function of roughness, observed in various systems by Dettre and Johnson (1964), has been interpreted along these lines: When we increase the roughness, we first find a normal increase of the barrier heights and a corresponding decrease of θ_r; but when the troughs become deep enough, we obtain a composite structure, with weaker barriers, and θ_r increases.

Note, finally, that the groove systems show an extremely strong anisotropy. When the line $\mathscr{L}$ is parallel to the grooves, it is pinned. When $\mathscr{L}$ lies (on the average) at a certain angle ψ from the grooves, it has the local structure shown in Fig. 11, and $\mathscr{L}$ can be displaced continuously

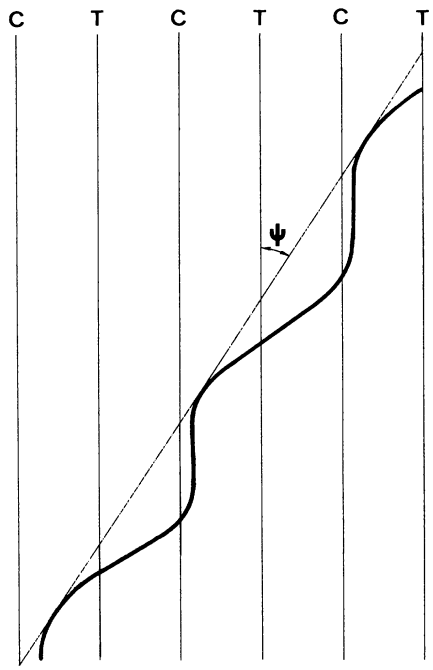

FIG. 11. A triple line $\mathscr{L}$ at an oblique angle (ψ) from a system of grooves (the crests and troughs are marked C and T, respectively). The overall pattern can be translated along the groove direction without any energy change (no pinning).

without any pinning (Cox, 1983). Experiments have been carried out for the special case $\psi=90°$ and indeed show no pinning (Mason, 1978).

In fact, the cascade of "jogs" displayed in Fig. 11 also gives us a hint about the physical processes that take place when $\mathscr{L}$ is parallel to the grooves ($\psi=0$). At $\psi=0$ the line wants to jump from one crest ($\mathscr{L}_1$) to the next ($\mathscr{L}_2$), as explained in Fig. 9(a). But the optimal method of doing this is not an overall jump (which would correspond to a huge barrier energy). What should really happen (in an infinite sample, with no edge effects) is shown in Fig. 9(b): nucleation of two "jogs" of opposite sign, followed by a glide of each jog along the grooves, until the ($\mathscr{L}_2$) strip spans the whole crest. Thus the physical barrier energy is independent of sample size, and is related to the nucleation and depairing of two adjacent jogs.

This statement holds when the grooves are infinitely long (or close on themselves, as they would in a capillary with grooves normal to the axis). If the grooves have a finite length (e.g., on a grooved plate), then a single jog may easily nucleate at the end of the groove and sweep through it. This process was discovered in recent numerical studies by Garoff and Schwartz (private communication).

3. Random surfaces

a. Weak fluctuations

A natural extension of the groove models is the case of surfaces that have a double periodicity, e.g., two orthogonal sets of grooves (Cox, 1983). However, it is clear that the major physical problem in this case corresponds to a random surface (random shape, or random chemical composition). This situation is, of course, more difficult. A first step, to make it simpler, is to focus on cases of *weak fluctuations*. To explain what this means quantitatively, let us start with a flat surface, but allow for chemical contamination. This will be described in terms of the local interfacial energies $\gamma_{SV}(x,y),\gamma_{SL}(x,y)$ at the point (x,y) on the surface. What matters is the difference $\gamma_{SV}-\gamma_{SL}$, or, more accurately, the fluctuating part

$$h(x,y)=\gamma_{SV}-\gamma_{SL}-\langle\gamma_{SV}-\gamma_{SL}\rangle\ , \tag{2.14}$$

where the angular brackets denote a space average. The local contact angle $\theta(x,y)$ at point (x,y) is given by the Young condition (2.1),

$$\gamma\cos\theta=h+\langle\gamma_{SV}-\gamma_{SL}\rangle\ , \tag{2.15}$$

while the unperturbed angle θ_0 is ruled by

$$\gamma\cos\theta_0=\langle\gamma_{SV}-\gamma_{SL}\rangle\ . \tag{2.16}$$

For small h we may thus write

$$\theta-\theta_0=-\frac{h(x,y)}{\gamma\sin\theta_0}\ , \tag{2.17}$$

and the condition for weak fluctuations is $|\theta-\theta_0|\ll\theta_0$ or, equivalently, $|\theta-\theta_0|\ll\sin\theta_0$, imposing

$$|h(x,y)| \ll \gamma \sin^2\theta_0 . \tag{2.18}$$

We shall assume that Eq. (2.18) holds in most of our discussion. This automatically eliminates certain interesting features (e.g., the "composite structures" mentioned earlier), but many important nonlinear effects are still present in this limit. [Remark: A further (convenient) simplification to be made here is to require that θ_0 itself be small, $\theta_0 \ll 1$. All calculations become simpler in this limit, without losing much physical content.]

Having defined weak fluctuations for chemical contamination, let us now turn to the case of surface roughness. Here the height of the interface at point (x,y) differs from the ideal value by a correction $u(x,y)$. We assume that the slopes $\varepsilon_x = \partial u/\partial x$, $\varepsilon_y = \partial u/\partial y$ are small. A systematic analysis of the effects to order ε^2 has been carried out by Cox (1983). Here we shall restrict our attention to the lowest significant order (ε). Let us define our axes (x,y) in the plane of average interface, so that the average contact line $\mathscr{L}$ is parallel to x. The "liquid side" is chosen to be the half-plane $y<0$ (Fig. 12). Then the major effect at any point is the rotation of the local surface, along an axis parallel to x, by an angle ε_y. The liquid/vapor interface makes an angle θ_0 with the tilted surface, but makes an angle

$$\theta = \theta_0 + \varepsilon_y = \theta_0 + \partial u/\partial y \tag{2.19}$$

with the average boundary plane (Fig. 12). Comparing Eqs. (2.19) and (2.17), we see that *the surface roughness problem and the chemical contamination problem coincide* (to first order in ε), provided that we set

$$-h(x,y) \leftrightarrow \gamma\theta_0 \partial u/\partial y \tag{2.20}$$

(for $\theta_0 \ll 1$).

The detailed statistical features of the random function $h(xy)$ depend on the particular system under consideration. In what follows, we shall restrict our attention to cases where $h(xy)$ is a random noise function with an amplitude h and a *finite* correlation range ξ. This is probably adequate for many types of chemical contamination and for certain forms of surface roughness (e.g., induced by abrasion). But the assumption may break down for certain special systems. For instance, as pointed out by Huse (private communication), if the solid is a glass, and if it has retained the thermal fluctuations of the surface it had as a melt, the surface $u(xy)$ is "rough" in the particular sense of statistical mechanics, and exhibits some anomalous long-range correlations.

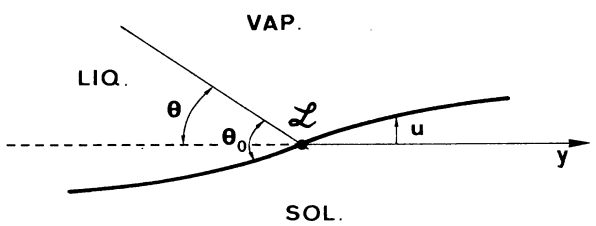

FIG. 12. Effect of a local tilt of the surface on the apparent contact angle θ.

b. The wandering triple line

Having defined the irregularities of the surface through a certain random function $h(x,y)$, we wish to understand how these irregularities react on the shape of the triple line $\mathscr{L}$. This has been attempted independently by Pomeau and Vannimenus (1984) and by Joanny and de Gennes (1984). The two approaches supplement each other, the first being more rigorous and the second giving certain physical insights.

A first step is to study a deformed line $\mathscr{L}$ [specified by a position $y=\eta(x)$ on the average surface] and to construct the elastic energy of the line. At first sight one might think of a line tension $\mathscr{T}$, giving an energy

$$f_{\rm el} = \int \tfrac{1}{2}\mathscr{T}\left[\frac{d\eta}{dx}\right]^2 dx$$

$$= \tfrac{1}{2}\mathscr{T}\sum_q q^2 |\eta_q|^2 , \tag{2.21}$$

where we have introduced the Fourier transform η_q of $\eta(x)$. The form (2.21) however, is wrong, and should be replaced by

$$f_{\rm el} = \tfrac{1}{2}\gamma\theta_0^2 \sum_q |q|\,|\eta_q|^2 . \tag{2.22}$$

Physically, the usual $|q|$ dependence for a mode of wavelength $2\pi/q$ expresses the fact that the line distortion perturbs the liquid/vapor interface on a thickness q^{-1}. Integrating a capillary energy (proportional to q^2) over this thickness, we get Eq. (2.22).

Let us now add the inhomogeneities described by $h(x,y)$. They contribute an energy

$$f_i = \int dx \int_{\eta(x)}^{\infty} dy\, h(x,y) . \tag{2.23}$$

We may equivalently say that $h = -\delta f_i/\delta\eta(x)$ is the local force f acting on the line $\mathscr{L}$,

$$f(x) = h[x,\eta(x)] . \tag{2.24}$$

We must now balance the elastic force [linear in the displacements $\eta(x)$] against the random force (2.24). But the random force is itself a (nonlinear) function of η. This point, emphasized by Pomeau and Vannimenus, makes the discussion quite delicate. Here, we shall use an illuminating presentation, due to Huse (1984), which parallels a classic idea of Imry and Ma (1975), improved later by Grinstein and Ma (1983) for the discussion of random field effects in ferromagnets. We consider a piece of line of macroscopic length l, which is pinned at both ends,

$$\eta(x=0) = \eta(x=l) = 0 . \tag{2.25}$$

Let us look for the ground-state energy of the line, assuming that it is characterized by a fluctuation amplitude

$$\eta(x) \sim W \quad (0<x<l) . \tag{2.26}$$

The corresponding elastic energy is derived from Eq. (2.22) with $q \sim l^{-1}$, and is

$$f_{el} \sim l \tfrac{1}{2}\gamma\theta_0^2 l^{-1} W^2 \cong \tfrac{1}{2}\gamma\theta_0^2 W^2 \ . \tag{2.27}$$

The energy f_i associated with the random force h can be estimated simply in two limits.

(i) If $W < \xi$ the line meets l/ξ uncorrelated inhomogeneities, each with random forces $\pm h$. The overall force is of order $\sqrt{l/\xi}h$, and the energy is

$$f_i \cong -Wh\sqrt{l/\xi} \ . \tag{2.28}$$

When this is added to Eq. (2.27), we find an optimum displacement

$$W \sim \frac{h}{\gamma\theta_0^2}\sqrt{l/\xi} \ . \tag{2.29}$$

This law has been quoted by Pomeau and Vannimenus (1984) and Joanny and de Gennes (1984a), but it is restricted to $W < \xi$, or, equivalently,

$$h < \gamma\theta_0^2\sqrt{\xi/l} \ . \tag{2.30}$$

(ii) If $W > \xi$, the line, when moving from its unperturbed position ($\eta = 0$), has swept a ribbon of area Wl, containing Wl/ξ^2 uncorrelated inhomogeneities. The resulting energy is

$$f_i \sim -h\xi^2(Wl/\xi^2)^{1/2} \sim -h\xi\sqrt{Wl} \ , \tag{2.31}$$

and the optimum W, obtained by minimization of $f_i + f_{el}$, is

$$W \sim \left[\frac{h}{\gamma\theta_0^2}\right]^{2/3} l^{1/3}\xi^{2/3} \ . \tag{2.32}$$

For most practical purposes, this second case is adequate, and the Huse formula (2.32) should hold. Taking $l = 1$ mm,[3] $h = \gamma\theta_0^2$, and $\xi = 1\ \mu$m, we get $W = 10\ \mu$m.

c. Line pinning

In the preceding section we considered only one (optimal) shape for the contact line $\mathscr{L}$. However, to describe hysteresis, we must compare different shapes. To understand the competition between two shapes, let us first consider a single "defect," following the arguments of Joanny and de Gennes (1984a). The word "defect" means a perturbation $h(x,y)$ localized near a particular point (x_d,y_d) and with finite linear dimensions $\Delta x \sim \Delta y = d$. Typical forms are shown in Fig. 13. The contact line $\mathscr{L}$ may have more than one equilibrium position near such a defect. In certain regimes it can become "anchored" to the defect as shown in Fig. 14. Far from the defect, the line coincides with $y = y_L$. Just on the defect ($x = x_d$), the line is shifted and reaches a certain value of $y = y_m$.

An essential parameter is the total force f_1 exerted by the defect on the line,

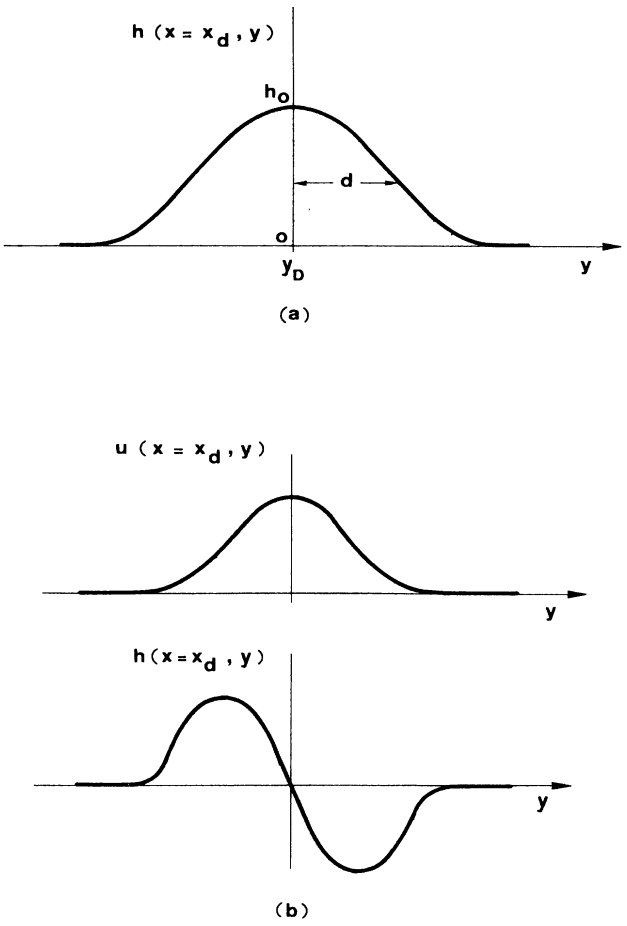

FIG. 13. Examples of smooth defect structures: (a) a chemical contaminant localized near one point (x_d,y_d) creates a localized peak in $h(xy)$; (b) a bump on the surface, described by $u(xy)$, induces an h function proportional to the derivative $\partial u/\partial y$.

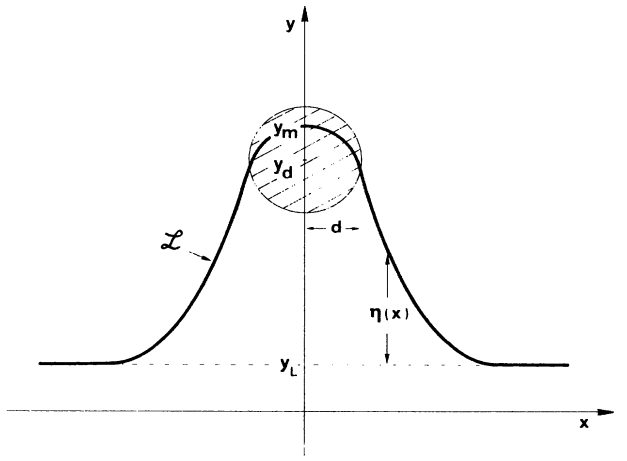

FIG. 14. A contact line $\mathscr{L}$ anchored on a defect. The defect is restricted to a small region (of diameter d), but the line is perturbed much farther out.

[3]This is an upper limit. Beyond that size gravitational energies come into play.

$$f_1 = \int_{-\infty}^{\infty} dx\, h[x, y_L + \eta(x)] \,. \tag{2.33}$$

The integral (2.33) is dominated by the central region $[x \sim x_d,\ \eta(x) \sim y_m - y_L]$ and will be approximated by the simpler form

$$f_1(y_m) = \int_{-\infty}^{\infty} dx\, h(x_1 y_m) \,. \tag{2.34}$$

For a given defect structure, $f_1(y_m)$ is then a known function of $y_m - y_d$ (Fig. 15). A simple example, to which we shall sometimes refer, is a Gaussian defect

$$h(x,y) = h_0 \exp\left[-\frac{(x-x_d)^2 + (y-y_d)^2}{2d^2} \right] . \tag{2.35}$$

In this case the force $f_1(y_m)$ is also Gaussian:

$$f_1(y_m) = (2\pi)^{1/2} h_0 d \exp\left[-\frac{(y_m - y_d)^2}{2d^2} \right] . \tag{2.36}$$

Let us now consider the line tip ($x = x_d, y = y_m$). The line here is in equilibrium under two forces, the force f_1 defined in Eq. (2.34), and an elastic restoring force, which tends to bring y_m back to the unperturbed line position y_L. This elastic force can be derived from the elastic energy (2.22). It has the simple Hooke form

$$f_{\rm el} = k(y_L - y_m) \,, \tag{2.37}$$

where k may be called the *spring constant of the line* and is given by

$$k = \frac{\pi \gamma \theta_0^2}{\ln(l/d)} \,. \tag{2.38}$$

Here l is a long-distance cutoff (for the single-defect problem, l would be the total length of line available), and d is always the defect size. The nice feature of Eq. (2.38) is that k is nearly independent of all defect properties. The balance of forces then gives the fundamental equation

$$k(y_m - y_L) = f_1(y_m) \,, \tag{2.39}$$

which is solved graphically in Fig. 15. When the strength of the defect [measured by h_0 in Eq. (2.35)] is small, there is only one root y_m for any specified y_L; we have no hysteresis. On the other hand, when the strength h_0 is beyond a certain threshold, we can find three roots (for a certain interval of y_L values); then we expect hysteresis.

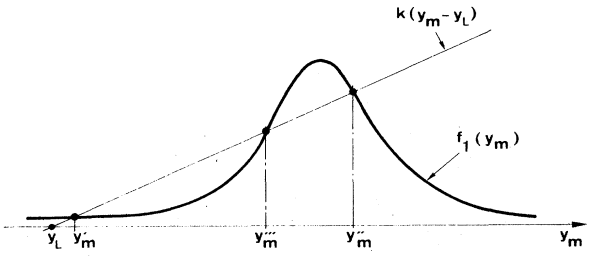

FIG. 15. Equilibrium positions for the anchoring point ($y = y_m$) of the line on the defect. The position of the line far from the defect is imposed ($y = y_L$). For a given y_L there may be three equilibrium positions; two of these (y'_m, y''_m) are locally stable.

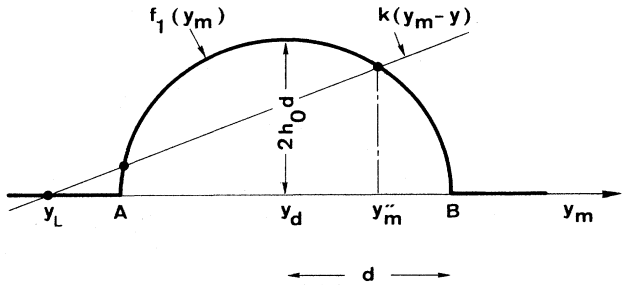

FIG. 16. An example of a "mesa" defect. The function $h(x_g)$ is zero, except in a circle of radius d around the point $(x_d y_d)$, where it is constant ($h = h_0$). Then the force $f_1(y_m)$ has the aspect shown. Even for very weak h_0 there exist two competing equilibrium positions (at y''_m and y_L), when y_L is just to the left of point A: hysteresis is always present.

This brings us to a very important conclusion for "regular" defects, i.e., for cases when $f_1(y_m)$ is a smooth function [with a finite derivative $f'_1(y_m)$]. We see that weak perturbations create strictly no hysteresis: to have a good determination of the thermodynamic angle θ_e, we do not need an ideal surface; we need only a surface with irregularities below a certain threshold.

The case of "mesa" defects (where the function h has step discontinuities) is completely different (Fig. 16). With mesa defects we can have hysteresis even for very small h functions. (Mesa structures can be obtained, for instance, with fatty acids on glass; see Brockway and Jones, 1964.) The mesa case was the only one considered by Pomeau and Vannimenus (1984). For this reason, some of their conclusions on the magnitude of the macroscopic hysteresis are somewhat specialized.

Up to now we have discussed only a single defect. It is not too hard, however, to extend the arguments to a *dilute* system of defects, and to produce detailed formulas for the hysteresis parameters θ_a and θ_r (Joanny and de Gennes, 1984a). The only nontrivial point in this extension is a renormalization of the spring constant k [Eq. (2.38)]: here the cutoff length l becomes the average distance between defects, as seen by the line $\mathscr{L}$. If n is the number of defects/cm^2,

$$l \to (nd)^{-1} \,.$$

There is good hope of comparing these predictions with experiments performed on *controlled defects,* with sizes in the 10-μm range.[4] They can be prepared by film deposition, using the many techniques currently in use in microelectronics. One can arrange to have either diffuse edges ("regular" defects) or sharp edges ("mesa" defects), and one can purposely locate these defects at random on a

[4]At much smaller sizes (below 1000 Å) the barriers between the equilibrium positions may be overcome by thermal agitation.

given surface. Measurements of contact angles in such systems should provide much more information on the basic laws of hysteresis.

d. Effects of inhomogeneities in situations of complete wetting

The above discussion was concerned with cases where $S<0$ (partial wetting), allowing for finite contact angles. What happens in the opposite case, where S is positive (complete wetting) but varies from point to point? This has been discussed recently (de Gennes, 1984e). It turns out that the final state of a droplet in dry spreading can be quite complex. The regions of high S are wet, while the regions of low S are not. The final thickness $\bar{e}$ of a *macroscopic* droplet adjusts itself so that the dry "islands" are just at their percolation threshold (i.e., at the onset of a continent). These considerations also suggest that many hysteretic effects could take place in dry spreading, but (to the author's knowledge) we do not have any experimental observations in this regime.

D. Wetting films and contact lines

1. Role of long-range forces

All our previous discussion dealt with macroscopic scales (larger than 1 μm). We now want to investigate smaller scales (say from 30 Å to 1 μm), where a continuum picture is still applicable, but where certain long-range forces become relevant, mainly van der Waals (VW) forces for organic liquids, or double-layer forces for water. (Classical reviews on these forces were given long ago by Dzyaloshinskii *et al.*, 1961; Overbeek and Van Silfhout, 1967; and Lyklema, 1967). Let us call $P(\zeta)$ the long-range tail of the energy/cm^2 of a flat liquid film of thickness ζ, lying on the solid. It is related to the celebrated "disjoining pressure" $\Pi(\zeta)$ introduced by Deryagin (1940) and reviewed in Deryagin (1955; see also Deryagin and Churaev, 1976), via $\Pi=-dP/d\zeta$,

$$P(\zeta)=\int_{\zeta}^{\infty} d\zeta' \Pi(\zeta') \ . \tag{2.40}$$

A lucid discussion of our present knowledge of the function $\Pi(\zeta)$, for various liquids and various substrates, and of its application to dynamical studies has been given by Teletzke, Davis, and Scriven (1984). In what follows we extract only some relatively simple limiting cases.

a. van der Waals forces

Here we have two regimes:

$$P(\zeta)=\begin{cases} A/(12\pi\zeta^2) & (\zeta<\lambda\text{; nonretarded}) \quad (2.41) \\ B/(3\zeta^3) & (\zeta>\lambda\text{; retarded}) \ . \quad (2.42) \end{cases}$$

We shall restrict our attention to the case where the constants A and B are positive. This means that VW forces tend to thicken the liquid film (the "agonist" case in the nomenclature of de Gennes, 1983). The crossover length $\lambda=\lambda/2\pi$ is roughly related to a characteristic ultraviolet absorption wavelength λ of the medium, and is of order 800 Å.

b. Double-layer forces

If the liquid L is water, or more generally an ionic solution (of screening length κ_D^{-1}), the solid will usually create in the water a charge double layer, of thickness κ_D^{-1}. Since water has a high dielectric constant $\varepsilon\cong 80$, while the vapor phase has $\varepsilon\cong 1$, the electric field must (nearly) vanish at the liquid/gas interface. This means that the double layer is repelled by an electrostatic image. The asymptotic form of this repulsion at large ζ was computed long ago by Langmuir (1938) and Frumkin (1938). The "disjoining pressure" Π is exponential,

$$\Pi=C\exp(-2\kappa_D\zeta) \quad (\kappa_D\zeta>1) \ , \tag{2.43}$$

where (for monovalent ions, such as Na^+ and Cl^-) the prefactor is

$$C=64nk_BT\tanh(\psi_0 e/k_BT) \ . \tag{2.44}$$

Here ψ_0 is the potential at the solid surface, n is the number of ions/cm^3 in the water, and e is the unit charge. Comparisons between Eqs. (2.43), (2.44), and ellipsometric data on water films have been carried out by Callaghan and Baldry (1978). They find that Eq. (2.44) does not give a very good fit to their data, and use some more complicated models.

In the regime $\kappa_D\zeta<1$ the experimental data are somewhat surprising. Pashley (1980) concludes that $\Pi(\zeta)\sim\zeta^{-1}$ (for water on glass or silica) in the region $\zeta<400$ Å. There is no obvious theoretical explanation for this slow decrease.

On the other hand, the data reviewed by Israelashvili (1982), on double-layer forces between two closely spaced mica plates, do agree with the standard theory and thus with Eq. (2.44), in the large thickness limit. In any case, to obtain simple predictions on thick wetting films and contact lines, the form (2.44) is a natural starting point.

2. Final spreading equilibrium

It will be much simpler to discuss a one-dimensional problem where the liquid thickness ζ depends only on one coordinate x in the plane of the solid surfaces (Fig. 17). The ingredients in the free energy are listed below:

$$f=f_0+\int_{x_{\min}}^{x_{\max}} dx\left[-S+\frac{\gamma}{2}\left[\frac{d\zeta}{dx}\right]^2+P(\zeta)+G(\zeta)\right] \ . \tag{2.45}$$

Here $(x_{\min},x_{\max})$ represent the interval covered by liquid. S is defined by Eq. (2.3) for the "dry" case, and by a similar rule (replacing γ_{SO} by γ_{SV}) for the "moist" case. The

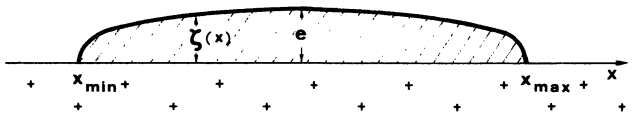

FIG. 17. The final "pancake" in complete dry spreading ($S>0$). Contrary to common belief, the equilibrium state is not a molecular film. Whenever $S \ll \gamma$ the thickness e is larger than the molecular size a.

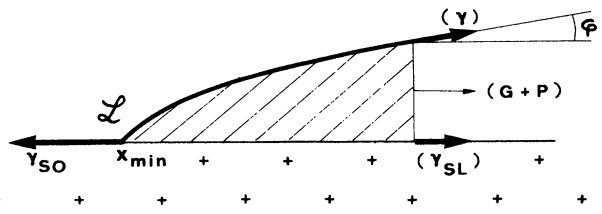

FIG. 18. The balance of forces on a liquid portion near the contact line $\mathscr{L}$.

γ term results from an expansion of the length element $ds^2=dx^2+d\zeta^2$, assuming $d\zeta/dx$ small (this will turn out to be the most interesting regime). The long-range forces show up in $P(\zeta)$. Note that $P(\zeta\to\infty)=0$. The interfacial energies S and γ appearing in Eq. (2.45) are the thermodynamic values, valid for thick films ($\zeta\to\infty$). They do incorporate contributions from the long-range forces. Finally $G(\zeta)$ describes gravitational and hydrostatic effects. These effects are often negligible for microscopic studies on contact lines and wetting films, but they show up in some special cases, and we keep them for this reason:

$$G(\zeta)=\rho g(\zeta^2/2+\zeta H)\ , \tag{2.46}$$

where ρ is the density difference between liquid and gas, g is the gravitational acceleration, and the H term has different meanings depending on the case being considered.

(a) For the "moist" case, the very existence of a liquid/vapor equilibrium requires that, in the experimental cell, a macroscopic reservoir of bulk liquid be present and in contact with the vapor. Then H is the difference in level between the solid plate and the liquid surface in the reservoir.

(b) For the "dry" case, the total volume of the spreading droplet, Ω, is fixed (no exchange), and we may think of the quantity

$$p_0=-\rho g H \tag{2.47}$$

as a Lagrange multiplier associated with this condition. After finding the droplet shape, imposing Ω fixes p_0.

The minimization of Eq. (2.45) with respect to $\zeta(x)$ leads to a standard equilibrium condition,

$$-\gamma\frac{d^2\zeta}{dx^2}+\frac{dP}{d\zeta}+\frac{dG}{d\zeta}=0\ , \tag{2.48}$$

which has an important first integral,

$$\frac{\gamma}{2}\left[\frac{d\zeta}{dx}\right]^2=P(\zeta)+G(\zeta)-S\ . \tag{2.49}$$

The value of the integration constant is best understood from the balance of horizontal forces shown in Fig. 18. Let us consider, for instance, a fluid region extending up to a value of ζ where long-range forces are negligible [$P(\zeta)=0$]. The fluid region experiences on the right the forces $\gamma\cos\varphi+\gamma_{SL}$ (capillary) and $G(\zeta)$ (hydrostatic). To the left we have the force γ_{SO}. Noting that

$$\cos\varphi\cong 1-\tfrac{1}{2}(d\zeta/dx)^2\ , \tag{2.50}$$

we recover (2.49). The calculation of all droplet shapes $\zeta(x)$ can now be performed by simple quadratures. We shall apply this scheme in the following section.

3. Partial wetting: microscopic structure of contact lines

a. Organic liquids: effects of van der Waals forces

Let us now consider the case of a nonzero contact angle θ_e ($\theta_e \ll 1$). In this case,

$$S=-\tfrac{1}{2}\gamma\theta_e^2 \tag{2.51}$$

is negative. We insert this value in Eq. (2.49) and discuss the core structure of the contact line $\mathscr{L}$.

In the vicinity of the contact line (Fig. 18) we may ignore gravitational forces as well as the macroscopic pressure difference p_0. Setting $G=0$ in Eq. (2.49), we then have

$$\left[\frac{d\zeta}{dx}\right]^2-\theta_e^2=2\gamma^{-1}P(\zeta)\ . \tag{2.52}$$

For most practical purposes here, the nonretarded form of $P(\zeta)$ [Eq. (2.44)] is adequate; we then define a molecular length a,

$$a^2=A/(6\pi\gamma)\ . \tag{2.53}$$

Solving Eq. (2.52) explicitly, we find a hyperbolic form,

$$\zeta^2=(\theta_e x)^2+(a/\theta_e)^2\ . \tag{2.54}$$

Results equivalent to Eq. (2.54) for $\zeta\gg a$ were first obtained by Berry (1974). See also Joanny and de Gennes (1984b). Of course Eq. (2.54) is meaningful only in the regions where $d\zeta/dx\ll 1$, or equivalently $\zeta\gg a$. But, for small contact angles θ_e, the hyperbolic profile extends to thicknesses $\zeta\sim a\theta_e^{-1}$, which can be of order 100 Å, and is thus significant.

The limiting case $\theta_e=0$ (complete wetting) should also be mentioned at this point. Integrating (2.52) for this case, we reach a parabolic shape,

$$\zeta^2=2a(x-x_L)\quad (a<\zeta<\lambda)\ . \tag{2.55}$$

Beyond λ we must switch to the retarded form for $P(\zeta)$,

and we find a slightly different exponent,

$$\zeta^5 = B\gamma^{-1}[\tfrac{5}{3}(x - x_L)]^2 \quad (\zeta > \lambda) . \tag{2.56}$$

Ultimately, when ζ gets large, the gravitational/hydrostatic terms $G(\zeta)$ come into play. One then returns to macroscopic physics (see Bouasse, 1924).

The profile for the opposite (and probably less frequent) case of *antagonist* VW forces ($A < 0$ and θ_e finite) has been discussed by Wayner (1982).

b. Water solutions: double-layer effects

If we insert Eq. (2.43) into Eq. (2.52), we find the modified wedge structure illustrated in Fig. 3(b): the local contact angle θ_1 near $\mathscr{L}$ tends to be larger than the thermodynamic angle θ_e. If we use Eq. (2.43) down to low values of the thickness ζ, we get

$$\theta_1^2 - \theta_e^2 = \frac{2P(0)}{\gamma} = \frac{2C}{\kappa_D \gamma} \quad (\theta_1 < 1) . \tag{2.57}$$

Equation (2.57) is only indicative. In actual fact, at small ζ the exponential form (2.43) does not hold, and the VW terms may play a role as well. But, independently of these details, the perturbation around $\zeta = \kappa_D^{-1}$, indicated in Fig. 3(b), is meaningful.

Here again, the special case of complete wetting deserves a special mention. For $\theta_e = 0$, Eq. (2.52) gives a logarithmic profile:

$$\zeta = \kappa_D^{-1} \ln[1 + x\kappa_D^{3/2}(\gamma/C)^{1/2}] . \tag{2.58}$$

Just as in the case of van der Waals forces, this holds only in the microscopic regime. Ultimately, at large ζ, the gravitational and hydrostatic terms become dominant, and we return to standard macroscopic forms.

4. "Complete" spreading: thickness of the wetting films

a. The "moist" case

A horizontal plate (at height H above reservoir level) is exposed to the vapor and completely covered by a wetting film. Here there does not exist a contact line giving us a balance of forces and specifying the integration constant in Eq. (2.49). But we obtain directly the equilibrium thickness e by minimization of van der Waals and gravitational energies:

$$\Pi(e) = \rho g (e + H) . \tag{2.59}$$

This is a classical equation, discussed long ago by the Russian school (Deryagin, 1940; Dzyaloshinskii *et al.*, 1961), verified on Rollin films of He_4 (Brewer, 1978), on normal fluids (Deryagin *et al.*, 1978), and somewhat less clearly verified in experiments with consolute mixtures near the free surface (see the review by Moldover and Schmidt, 1983). Basically, when H is macroscopic (~ 1 cm) the thickness is small ($e \sim 300$ Å), and nonretarded interactions often prevail. On the other hand, the limit $H = 0$ does not seem to have been experimentally explored (it could be easily controlled by interference techniques). It would lead to very thick films ($e \sim 10$ μm) and to a rather direct determination of retarded VW forces:

$$e(H = 0) = (B/\rho g)^{1/5} . \tag{2.60}$$

b. Nonvolatile liquids (the "dry" case)

Here a spreading droplet ultimately becomes a flat "pancake," and we want to determine (i) the thickness of the pancake, and (ii) some information on the structure near the contact line (Fig. 17). For our one-dimensional problem the shape is ruled by Eq. (2.49), with $S > 0$. The maximum thickness corresponds to $d\zeta/dx = 0$, and this gives a condition

$$P(e) + G(e) = S . \tag{2.61}$$

But we have two unknowns: the thickness e and the pressure p_0. To obtain a second condition, for a finite droplet, we should calculate the total volume Ω. Here, however, we shall restrict our attention to the limit of a very wide pancake ($\Omega \to \infty$). As usual, it is then convenient to think of Eq. (2.49) as the conservation of energy for a classical particle of position ζ at time x, with a mass γ, a potential energy $-(P + G)$, and a total energy $-S$.

For strongly negative values of the total energy $-S$, the particle oscillates in a wall near $\zeta = 0$, and the period is finite (i.e., the droplet size is finite). But if $-S$ is adjusted to coincide with the maximum of the potential, then the particle takes an infinite time to reach this maximum (infinitely wide pancake). The maximum then defines the position at long times (the macroscopic thickness of the pancake). This gives a hydrostatic condition identical in form to Eq. (2.59),

$$\Pi(e) = \rho g (H + e) , \tag{2.62}$$

where $\Pi = -dP/de$ is always the disjoining pressure. Eliminating (H) between Eqs. (2.61) and (2.62), we obtain an explicit relation between the spreading coefficient S and the wetting film thickness:

$$P(e) + e\Pi(e) - \tfrac{1}{2}\rho g e^2 = S . \tag{2.63}$$

To discuss Eq. (2.63), let us restrict our attention to van der Waals forces, with the simple limiting forms (2.42) or (2.43),

$$P(e) \sim e^{-m} , \tag{2.64}$$

$$P(e) + e\Pi(e) = (m + 1)P(e) . \tag{2.65}$$

We start from $S \to 0$: here, the thickness e is large, and we must use the retarded form ($m = 3$). This gives

$$S = 4B/3e^3 - \rho g e^2/2 . \tag{2.66}$$

The wetting film thickness at $S = 0$ is

$$e(S = 0) = e^* = (8B/3\rho g)^{1/5} , \tag{2.67}$$

differing only by a numerical coefficient from the thickness at $\theta_e=0$ in complete equilibrium [Eq. (2.60)]. Typically e^* equals several micrometers. If we now turn to small, positive values of the spreading coefficient S, we see from Eq. (2.66) that a useful dimensionless parameter is

$$u=S(e^*)^3/B \ . \tag{2.68}$$

Numerically $B/(e^*)^3\sim 10^{-7}$ ergs/cm^2, while $S\sim 0.1$ erg/cm^2. Thus u is immediately very large. Consequently, the gravitational term in Eq. (2.67) becomes completely negligible, and we may write (2.65) in the form

$$S=e\Pi(e)+P(e) \ . \tag{2.69}$$

Equation (2.69) is the basic formula for dry spreading with finite S. It could be obtained more directly by ignoring the edge of the "pancake" and writing only the extensive part of the energy. If $\mathscr{A}$ is the pancake area, this is a sum of capillary and VW energies,

$$f=f_0-S\mathscr{A}+\mathscr{A}P(e) \ . \tag{2.70}$$

This must be minimized with the constraint

$$e\mathscr{A}=\Omega=\text{const} \ , \tag{2.71}$$

which brings one directly to Eq. (2.69).

For most practical purposes (finite S), the value of e deduced from Eq. (2.69) is of order 100 Å or less. The nonretarded form of VW interactions holds ($m=2$). This gives the final formula (Joanny and de Gennes, 1984b)

$$e=a\left[\frac{3\gamma}{2S}\right]^{1/2} \quad (a<e<\tilde{\lambda}) \ . \tag{2.72}$$

Equation (2.72) provides the explanation for a very classical fact, observed long ago by Cooper and Nuttal (1915): liquids of large S spread more efficiently than liquids of small S. We do see in Eq. (2.72) that the final spreading film is thinner if S is larger, and this, in turn, implies that the equilibrium surface covered is larger.

Most of us believed that the explanation of the Cooper-Nuttal rule could be based on a different, dynamic effect, namely, more rapid spreading of drops of large S, but this is not true. As we shall see in Sec. IV, the rate of spreading of a droplet is essentially *independent of* S.

Let us close this discussion with two remarks. The first concerns the *edge* of the "pancake" realized after spreading. Returning to the minimization near $\zeta=0$, we can check that the edge is always parabolic, with the structure (2.55).

The second remark concerns the case where the dominant long-range force is due to a double layer. Then, neglecting gravitational effects and inserting (2.43) into (2.69) one arrives at

$$e=\frac{1}{2\kappa_D}\ln\left[\frac{C}{S\kappa_D}\right] \ . \tag{2.73}$$

Equation (2.73) should hold for $S\ll C\kappa_D^{-1}$. At larger values of S, the discussion should include both VW and double-layer forces, and becomes more complex.

c. Complete wetting: vertical wall

The macroscopic analysis for a wetting liquid ($\theta_e=0$) near a *vertical* wall predicts a certain curved profile, with a contact line $\mathscr{L}$ at a level h_1 above the bulk liquid surface,

$$h_1=\sqrt{2}\kappa^{-1} \tag{2.74}$$

(see Bouasse, 1924). Here κ^{-1} is a capillary length (not to be confused with the Debye screening length κ_D^{-1}) of order of magnitude 1 mm. We have

$$\kappa^2=g\rho\gamma \ . \tag{2.75}$$

How is this modified when we switch on the VW forces? For $S=0$ exactly, the picture is essentially unaltered. For $S>0$, a film climbs up the wall. If x is now the altitude above the bulk liquid surface, and $\zeta(x)$ the film thickness, the equilibrium condition is (in the nonretarded regime)

$$\frac{d^2\zeta}{dx^2}+\frac{a^2}{\zeta^3}-\kappa^2 x=0 \ . \tag{2.76}$$

The standard (loose) discussion of Eq. (2.76) separates out two regimes.

(i) *The film regime,* where the curvature term $d^2\zeta/dx^2$ is negligible, leaving an exact balance between VW and gravitational pressures:

$$\zeta=\zeta_1(x)=x^{-1/3}\kappa^{-2/3}a^{2/3} \ . \tag{2.77}$$

[It has been realized recently (Joanny and de Gennes, 1984c) that the profile (2.77) does not hold up to arbitrarily large altitudes x. Returning to the full equation (2.76), one can show that the film is *truncated* at a certain $x=x_m$, such that $\zeta_1(x_m)=e(S)$, where $e(S)$ is the minimal thickness defined in Eq. (2.72).]

(ii) *The macroscopic regime,* where the VW forces are negligible.

The crossover between (i) and (ii) is nontrivial; it was discussed long ago by Deryagin (1940),[5] more recently by Renk, Wayner, and Homsy (1978), Adamson and Zebib (1980), and by Telo de Gama (unpublished), Legait and de Gennes (1984), and Evans and Marini (1985) in connection with experiments by Moldover and Gammon (1983) who were studying capillary rise between *two* plates. Moldover and Gammon had proposed that the effective interplate distance (to compute the capillary rise) be reduced by twice the thickness of a single film, $2\zeta_1(x_l)$, taken at the level of the nominal contact line $x=x_l$. Actually the presence of a second plate thickens the films, and the correction should be $3\zeta_1(x_l)$ rather than $2\zeta_1$ (in the

[5] I am indebted to Professor R. Evans for the Deryagin reference.

nonretarded regime). Similarly, for a single plate, the thickness of the film in the crossover region ($x_l \sim h_1$) is expected to be

$$\zeta \sim \zeta_1(h_1) \sim \kappa^{-1/3} a^{2/3} . \tag{2.78}$$

Finally let us consider the case of negligible van der Waals forces and dominant double-layer forces. Equilibrating gravitational pressures and double-layer pressures, we get a thickness

$$\zeta(x) = \frac{1}{2\kappa_D} \ln \left[\frac{B}{\rho g x} \right] , \tag{2.79}$$

and we find a film extending up to a finite height,

$$x_m = \frac{B}{\rho g} . \tag{2.80}$$

Equation (2.79) is limited by the restrictions mentioned after Eq. (2.58): above $x = x_m$ a residual film may be present, because of short-range disjoining pressures, but below $x = x_m$ the logarithmic profile should be visible.

III. THE WETTING TRANSITION

A. Experiments on related systems

1. Scope

A liquid/vapor interface L/V, in the vicinity of a solid S, may exhibit either a finite equilibrium contact angle θ_e (partial wetting) or a strictly vanishing contact angle (complete wetting). There may exist a particular temperature T_w at which we switch from one regime to the other. This is called the wetting transition temperature.

Unfortunately, the $L/V/S$ systems are usually not convenient for studies of this wetting transition. To change significantly the interfacial energies γ_{ij}, we would have to scan a rather broad temperature range. To maintain the L/V equilibrium then requires that one work at high pressures. Because of these practical difficulties, all current studies on T_w have been carried out with the other three-phase equilibria, where temperature variations (at atmospheric pressure) are feasible and have more spectacular effects on the interfacial energies. The two main examples are solid/liquid A/liquid B, free surface/liquid A/liquid B, where A and B are two coexisting phases of a binary mixture with a certain critical consolute temperature T_c. It turns out that, for such a case, the interfacial energies vary considerably when we consider the broad vicinity of T_c (typically a 30° interval). This makes the experimentation much simpler.

Thus, in this section, we shall broaden our subject and consider a variety of three-phase equilibria. The main emphasis, however, will be on solid/fluid/fluid systems. It is reasonable to assume that all these systems are rather similar (as far as the *static* properties are concerned). Thus the liquid/vapor wetting transitions, when observed, will probably follow the laws described here.

2. Wetting films

Numerous examples of complete wetting are found with solid/liquid/vapor systems. But the existence of wetting films, with $\theta_e = 0$, in other types of three-phase equilibria has been established only during the last decade.

An important, early experiment was carried out by Heady and Cahn (1972). Here the solid S is replaced by a vapor phase. The analogs of L and V are two liquids, made of a hydrocarbon (methyl cyclohexane) and of the fluorinated analog of this hydrocarbon. The fluorocarbon (hydrocarbon) system has a consolute point T_c. Below the critical temperature T_c we can have coexistence of two equilibrium phases; one of these is rich in fluorocarbon and will be called L; the other is rich in hydrocarbon and will be called V.

The original aim of the Heady-Cahn experiment was to study a quench into the two-phase region, followed by nucleation of L into V. They found, however, that, in the vicinity of the free surface, nucleation barriers could never be observed: droplets of L immediately began to drip from the surface. They concluded that, in the range of temperatures studied, a wetting film of L was always present near the surface S.

Another early observation of wetting films came from metallurgy (Zabel *et al.*, 1981). The L/V system here is a single crystal of niobium containing a significant fraction of dissolved hydrogen. The analog of S is again the free surface. In a certain temperature range the Nb/H system shows a two-phase equilibrium ($\alpha \leftrightarrow \alpha'$). Both phases are cubic, but they differ in their hydrogen content. The lattice spacing is swollen by the presence of H, and the nature of the phase present near the surface can thus be detected by x-ray reflections. The conclusion is that the α phase wets the interface, the thickness of the α film being of order one micron.

3. Wetting transitions with consolute pairs

A relatively simple measurement of θ_e was carried out by Pohl and Goldburg (1982) on a system of two liquid phases (A,B) (lutidine water mixtures) against common glass (S). The technique is based on capillary rise (Fig. 4) and allows for a plot of $\cos\theta_e$ as a function of temperature. Below a certain temperature $T = T_w$, $\cos\theta_e = 1$, while above $T = T_w$, $\cos\theta_e$ decreases (with a nearly constant slope).

Another important measurement was carried out by Moldover and Schmidt (1983) with S=free surface, A,B=alcohol + fluorocarbon mixtures. Macroscopic measurements of the contact angle indicated a wetting transition at $T_w = 311$ K, and complete wetting (by the fluororich phase) in the interval between T_w and $T_c = 363$ K. Ellipsometric measurements of the thickness e of the fluorocarbon film show a finite jump of $e(T)$ at $T = T_w$. This transition is clearly of first order.

To summarize, for these $S/A/B$ systems we find complete wetting in a finite temperature interval (T_w, T_c) near the critical point, and partial wetting far from T_c. There

are more complicated cases. In particular, the pair cyclohexane-methanol, near the free surface S, shows a complex sequence of transitions, which occurs only in the presence of dilute contaminants (water, acetone). We shall come back to these impurity effects at the end of Sec. III.B. But the two examples (Pohl and Goldburg, 1982; Moldover and Schmidt, 1983) above are probably typical of a generic (impurity-free) situation.

A final remark: wetting transitions are also observed with solid films evaporated on a solid surface (for instance, organic solids on graphite, or oxygen on graphite). But the situation here is more complex for many reasons. For crystalline, epitaxial films, the discrete nature of the solid layers introduces a wealth of new transitions, and the elastic distortion fields induced by the substrate complicate the energy balance. For a recent discussion of these "solid on solid" problems see Gittes and Schick (1984).

B. Theory

1. The Cahn model

We follow first the simple and illuminating arguments of Cahn (1977) phrased in language adequate for a solid/liquid/vapor system.

(a) The first simplification is to describe the liquid/solid interface by a *continuum theory*, where the liquid number density $\rho(z)$ varies smoothly as a function of the distance z from the solid surface (see Fig. 21 below). This will be most adequate if we are dealing with temperatures T that are not too far from the critical point T_c. The hope is that most variations of $\rho(z)$ will take place over distances comparable to the correlation length ξ, and this ξ is larger than the intermolecular distance (a) in the liquid, when $T \sim T_c$.

(b) A second, important assumption is that the forces between solid and liquid are of *short range* ($\sim a$), and can, in fact, be described simply by adding a special energy $\gamma_c(\rho_s)$ at the solid surface. Here $\rho_s = \rho(z=0)$ is the liquid density "at the surface" and γ_c is a certain functional,

$$\gamma_c = \gamma_0 - \gamma_1 \rho_s + \tfrac{1}{2}\gamma_2 \rho_s^2 + \cdots \ . \tag{3.1}$$

The γ_1 term (favoring large ρ_s) describes an attraction of the liquid by the solid. The γ_2 term represents a certain reduction of the liquid/liquid attractive interactions near the surface: a liquid molecule lying directly on the solid does not benefit from the same high number of liquid neighbors that it would have in the bulk. The parameters γ_1 and γ_2 describe the essential features at the interface. However, the Cahn approach is slightly more general than Eq. (3.1): any form of $\gamma_c(\rho_s)$ is acceptable. We may say that γ_c is the contribution to the solid/fluid interfacial energy which comes from direct contact. This is not all the interfacial energy. Another contribution γ_d will come from the distortions in the profile $\rho(z)$.

(c) A final (less important) approximation amounts to treating the fluid statistics by a mean-field theory. The specific form chosen for the free energy γ_d is a classical "gradient square" functional,

$$\gamma_d = \int dz \left[\tfrac{1}{2} L \left(\frac{d\rho}{dz} \right)^2 + W(\rho) \right] , \tag{3.2}$$

$$W(\rho) = F(\rho) - \rho\mu - P \ . \tag{3.3}$$

Here F is the free-energy density of the bulk liquid, μ its chemical potential, P its pressure. [For a complete justification of Eqs. (3.2) and (3.3) see Rowlinson and Widom, 1982.] We shall assume that μ and P correspond to the exact coexistence of liquid and vapor. Then $W(\rho)$ has two minima of equal height ($W=0$) for the two equilibrium densities $\rho=\rho_l$ (liquid) and $\rho=\rho_v$ (vapor). The general aspect of $W(\rho)$ is shown in Fig. 19. For simplicity we take L independent of ρ.

2. Determination of the surface density

To construct the density profile in the liquid $\rho(z)$ we optimize (3.2) and obtain

$$-L\frac{d^2\rho}{dz^2} + \frac{dW(\rho)}{d\rho} = 0 \ , \tag{3.4}$$

from which we construct a first integral

$$\tfrac{1}{2}L\left(\frac{d\rho}{dz}\right)^2 = W(\rho) \ . \tag{3.5}$$

There is no integration constant in Eq. (3.5). If we consider a point far in the bulk, where $\rho=\rho_b$ (ρ_b being either ρ_l or ρ_v), we must have $d\rho/dz=0$ and $W(\rho_b)=0$ as explained in Fig. 19. The simple form of Eq. (3.5) allows for a direct calculation of the distortion energy γ_d [Eq. (3.2)],

$$\gamma_d(\rho_s\rho_b) = \int_{\rho_b}^{\rho_s} L\frac{d\rho}{dz}d\rho = \int_{\rho_b}^{\rho_s} [2LW(\rho)]^{1/2}d\rho \ . \tag{3.6}$$

The last step is to determine the surface density ρ_s by minimization of the total energy $\gamma_{\rm tot} = \gamma_d + \gamma_c(\rho_s)$. The resulting condition is

$$-\gamma_c'(\rho_s) = [2LW(\rho_s)]^{1/2} \tag{3.7}$$

[where $\gamma_c'(\rho) = d\gamma_c/d\rho$]. This leads to the graphical con-

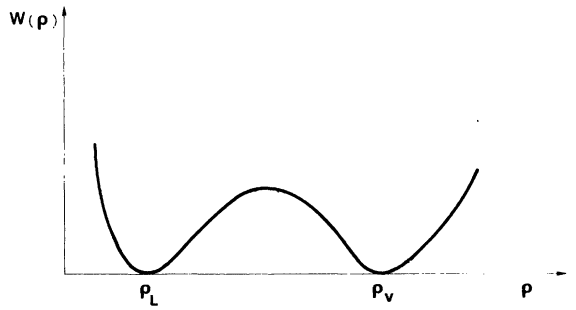

FIG. 19. The "effective free energy" $W(\rho)$ as a function of the density ρ.

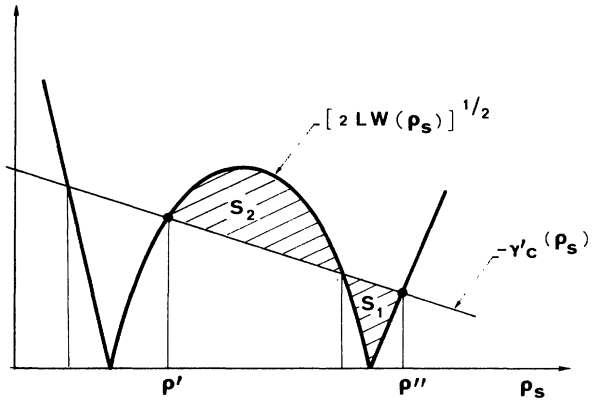

FIG. 20. The Cahn construction determining the density at the surface ρ_s. In the example displayed we have two locally stable roots (ρ',ρ''). The other two roots are unstable.

struction of Fig. 20. Here, for simplicity, we have chosen the specific form of $\gamma_c(\rho_s)$ proposed in Eq. (3.1), and this gives a linear plot for $-\gamma'_c(\rho_s)=\gamma_1-\gamma_2\rho_s$.

3. Two types of wetting transitions

a. First-order transitions

If the slope (γ_2) is small, the condition (3.7) may give four roots for ρ_s. Two of these are locally stable, while the others correspond to a maximum of the free energy and are unstable. In this regime we find a competition between a state of low ρ_s $(\rho_s=\rho')$ describing a nearly "dry" solid in contact with the vapor $(\rho_b=\rho_v)$ and a state of high ρ_s $(\rho_s=\rho''>\rho_l)$ describing a wet solid in contact with the liquid $(\rho_b=\rho_l)$. The energies of these two states are (per cm^2 of solid surface)

$$\gamma_{sv}=\gamma_d(\rho_v,\rho')+\gamma_c(\rho')\ ,$$
$$\gamma_{sl}=\gamma_d(\rho_l,\rho'')+\gamma_c(\rho'')\ . \tag{3.8}$$

We must also remember that the liquid/vapor interfacial energy γ can be derived from the same analysis:

$$\gamma=\gamma_d(\rho_v,\rho_l)\ . \tag{3.9}$$

Let us discuss the "spreading coefficient" defined in Sec. II:

$$\gamma_{sv}-\gamma_{sl}-\gamma=S\ . \tag{3.10}$$

Using Eqs. (3.6), (3.8), and (3.9), one can check that S has a simple graphical interpretation in Fig. 20: $S=S_1-S_2$ is the difference of the two shaded areas.

Let us now vary the temperature, as indicated in Fig. 21.

(i) At $T\ll T_c$ the difference $\rho_l-\rho_v$ is large, and S_2 is larger than S_1. This gives $S<0$, i.e., $\cos\theta_e$ is finite (partial wetting).

(ii) If we raise T, the difference S_1-S_2 decreases and vanishes at a special temperature $T=T_w$. Here $S=0$ and $\theta_e=0$.

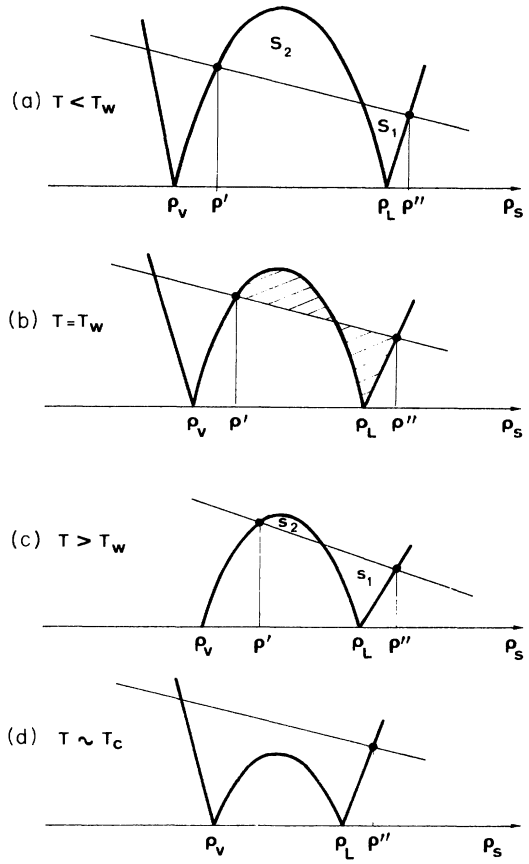

FIG. 21. First-order transition from the Cahn construction. (a) At low T, two surface states ρ' (solid/vapor) and ρ'' (solid/liquid) can exist. The spreading coefficient $S=S_1-S_2$ is negative (partial wetting). (b) At $T=T_w$, $S_1=S_2$ and the spreading coefficient vanishes. The contact angle is $\theta_e=0$. (c) At $T\gtrsim T_w$, $S_1>S_2$ and S is positive. But the low-density solution (ρ') is not observable in equilibrium. A wetting film is always lower in energy. (d) At higher T the root ρ' disappears completely: in this last regime it is not possible to define a spreading coefficient S.

(iii) At temperatures $T>T_w$, $S_2<S_1$, and S is positive. As we know from Sec. I, this regime is unobservable in thermal equilibrium. Instead of building up a liquid/vapor interface with $\rho_s=\rho'$, the system prefers to achieve it in two steps, through a macroscopic film of L wetting the surface and giving a total surface energy $\gamma_{sl}+\gamma$. Thus, here, we keep $\theta_e=0$ (complete wetting). Ultimately, at high temperatures ($T\sim T_c$), only one stable root is left, corresponding to a solid/liquid interface.

In this scenario the transition at T_w involves a jump from one energy minimum $(\rho_s=\rho')$ to a distinct minimum $(\rho_s=\rho'')$ and is clearly of *first order*. The plot of $\cos\theta_e$ versus temperature in the partial wetting regime has a finite slope, and intersects $\cos\theta_e=1$ at $T=T_w$.

b. Second-order transitions

If the slope (γ_2) of $-\gamma_c'(\rho_s)$ is large, at all temperatures T we find only *one root* ρ_s from the construction illustrated in Fig. 22.

(i) At low temperatures $\rho_s < \rho_l$, and we can construct two density profiles corresponding to two physical situations: one profile where $\rho(z)$ decreases from ρ_s to ρ_v (describing S/V) and one profile where $\rho(z)$ increases from ρ_s to ρ_l (describing S/L). Again a discussion of areas allows one to compare the surface energies. One finds a negative spreading coefficient, $S<0$ corresponding to partial wetting.

(ii) At high temperatures ($T > T_w$), the surface density ρ_s is higher than ρ_l; there is only one profile associated with ρ_s, where $\rho(z)$ decreases from ρ_s to ρ_l (S/L interface). The S/V interface must then involve a macroscopic film of L, and we have complete wetting. Clearly this scenario corresponds to a continuous ("second-order") transition. At $T=T_w$, $\rho_s=\rho_l$ exactly.

4. Special features of second-order transitions

Second-order wetting transitions are probably rather rare, for reasons to be explained below. But they have stimulated a considerable theoretical effort and deserve a few comments.

Let us consider a liquid film, of thickness ζ, covering the solid, and described by the density profile $\rho(z)$ shown in Fig. 23: most of the density drop takes place in a

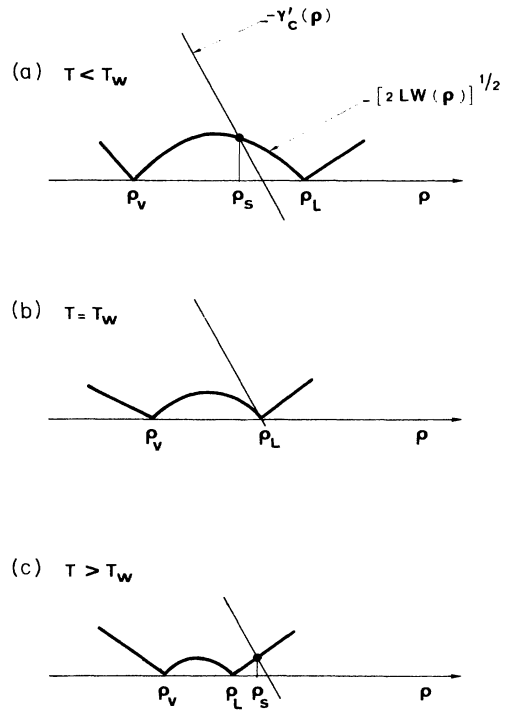

FIG. 22. Second-order transitions from the Cahn construction.

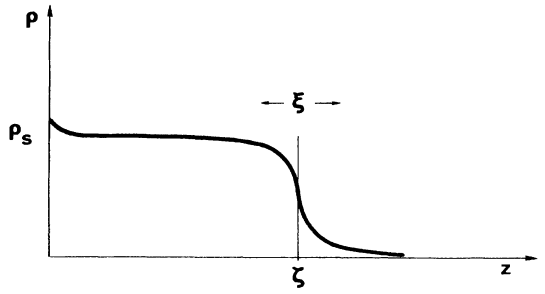

FIG. 23. Density profile for a thick film (thickness ζ larger than the interface width ξ). Depending on the coefficients in Eq. (3.1), the value at the surface (ρ_s) may be either larger or smaller than the bulk value in the liquid (ρ_L).

thickness ξ near the nominal interface (around $z=\zeta$). Far from this interface ($z \ll \zeta$) the difference between $\rho(z)$ and ρ_l is exponentially small. At the surface

$$\rho(z=0)=\rho_s=\rho_l-\varepsilon\ , \qquad \varepsilon \simeq (\rho_l-\rho_v)\exp-(\zeta/\xi)\ . \tag{3.11}$$

[Equation (3.11) can be derived from a complete integration of (3.5), taking for $W(\rho)$ the simplest polynomial form compatible with Fig. 19.] Near T_w (for T slightly lower than T_w) ε is small and positive, and the energy of the S/V interface may be expanded in powers of ε,

$$\gamma_{sv}=\gamma_{sv}(\varepsilon=0)-\alpha(T)\varepsilon+\tfrac{1}{2}\gamma_2\varepsilon^2+\cdots\ . \tag{3.12}$$

Here $\alpha(T)$ can be computed explicitly from Eq. (3.7) and is proportional to T_w-T ($\alpha>0$ for $T_w>T$). Equation (3.12) can be translated into a plot of film energy versus film thickness, since ε and ζ are related by (3.11):

$$\gamma_{sv}=\gamma_{sv}(T=T_w)-\alpha(\rho_l-\rho_v)\exp(-\zeta/\xi) + \tfrac{1}{2}\gamma_2(\rho_l-\rho_v)^2\exp(-2\zeta/\xi)+\cdots\ . \tag{3.13}$$

For $T<T_w$ we have a weak attractive tail at large ζ and a finite repulsive tail at smaller ζ (Fig. 24). There is an optimal film thickness which corresponds to $\varepsilon=\alpha/\gamma_2$ or

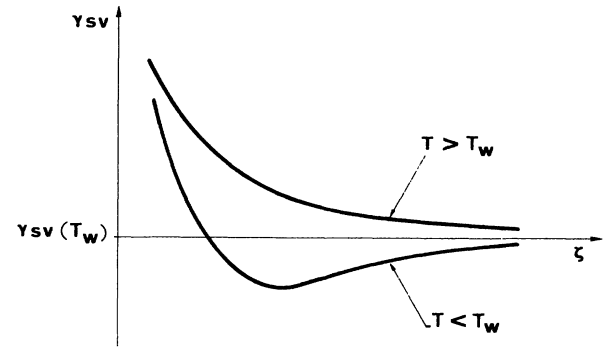

FIG. 24. Energy vs thickness for a film, in the vicinity of a second-order transition (at $T=T_w$). This type of plot (with exponential decay at large distance) would occur in the absence of long-range forces.

$$\zeta=\zeta^*=\xi\ln\frac{\gamma_2}{\alpha}\ . \tag{3.14}$$

This approach gives a very pictorial description of the second-order wetting transition (in a mean-field picture): there is a wetting film even for $T<T_w$, but its thickness diverges logarithmically at $T=T_w$. For $T>T_w$ the energy (3.13) becomes repulsive at all distances, and the film is macroscopic.

As usual, this mean-field picture is complicated by *fluctuation effects*. The L/V interface may undulate

$$\zeta(xy)=\zeta^*+u(xy)\ .$$

To order u^2 the fluctuation energy is

$$f=\int dx\,dy\left\{\gamma_{sv}(\zeta^*)+\tfrac{1}{2}\gamma''_{sv}(\zeta^*)u^2+\tfrac{1}{2}\gamma\left[\left(\frac{\partial u}{\partial x}\right)^2+\left(\frac{\partial u}{\partial y}\right)^2\right]\right\}, \tag{3.15}$$

where $\gamma''(\zeta^*)$ can be derived from Eq. (3.13) and turns out to be proportional to α^2. The form (3.15) leads to a correlation length ξ_u for the fluctuations:

$$\xi_u=\left[\frac{\gamma}{\gamma''(\zeta^*)}\right]^{1/2}\sim(T_w-T)^{-1}\ . \tag{3.16}$$

However, the expansion (3.15) of the energy to order u^2 is inadequate. If one computes from Eqs. (3.15) and (3.16) a mean-square average $\langle u^2\rangle$, one finds $u\sim\zeta^*$. Thus the special events where the fluctuating L/V interface touches the solid surface must be taken into consideration. This has been carried out in detail (Brézin, Halperin, and Leibler, 1983a,1983b) and gives rise to a very unusual critical exponent, whose value depends continuously on the parameter $kT_w/\xi^2\gamma$.

We shall not describe these delicate fluctuation effects in any detail, because they may often be short-circuited by long-range forces, as explained below.

5. Role of long-range forces

a. Simple estimates of wetting film energies

Let us assume that the short-range forces [described by $\gamma_c(\rho_s)$] lead by themselves to a second-order transition T_{w0} associated with the film energy (3.13). Then let us switch on an agonist van der Waals interaction, unretarded [Eq. (2.45)], with a positive Hamaker constant A. Then the plot of film energy versus thickness is still monotonous and repulsive for $T>T_{w0}$, and we have complete wetting in this temperature region. But for $T<T_{w0}$ the plot is deeply modified (Fig. 25). At large thicknesses ζ, the VW term dominates over the exponentials, and the energy is repulsive. At shorter distances the attractive exponential $-\alpha\exp(-\zeta/\xi)$ may create a trough when α is large enough. Finally, when α reaches a certain value α_1 (temperature T_1), the trough may give an energy equal to that of a macroscopic film $\gamma_{sv}(\zeta=\infty)$. At this point there is a certain optimal thickness ζ_1, and the system jumps by a first-order transition from $\zeta=\infty$ to $\zeta=\zeta_1$.

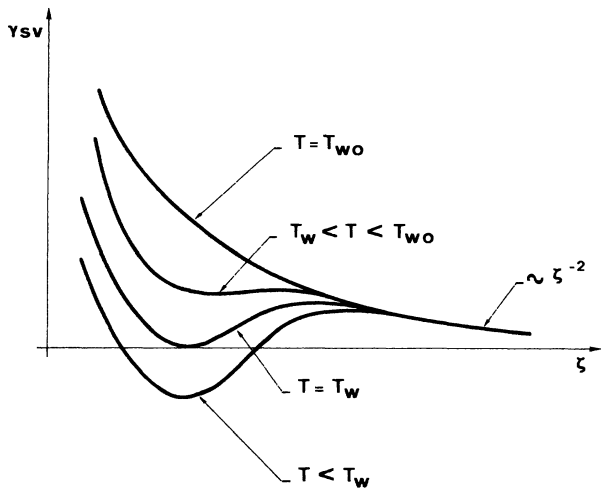

FIG. 25. Energy vs thickness with incorporation of long-range van der Waals forces. These forces are assumed to be "agonist" (i.e., they tend to thicken the film). They dominate at long distances.

A similar description can be given for water solutions against an ionizable surface. Whenever the Debye screening length κ_D^{-1} is larger than the L/V interface thickness ξ, the Langmuir repulsive term [obtained from Eq. (2.57)] dominates the behavior of the film energy at large distances, and the energy plot is qualitatively similar to the preceding one. The transition point is shifted from T_{w0} to a lower value T_1, and the transition becomes first order.

Finally let us mention briefly some other situations.

(i) An "antagonist" VW force, corresponding to a negative Hamaker constant A. Here the long-range energy tends to shrink the wetting film, and the L/V interface is thus stuck near the solid wall (partial wetting). A transition can, however, occur (at $T<T_{w0}$) between two different minima, corresponding, respectively, to a thick film and a thin film.[6]

(ii) When the density of the V phase varies significantly with temperature, it may happen that we switch from the agonist to the antagonist case at one particular temperature $T=T_S$ (Lipowsky and Kroll, 1984; Dietrich and Schick, 1984). If, in the absence of long-range forces, there were a second-order wetting transition at $T=T_{w0}$, then, upon switching on VW forces, one would still expect a second-order transition, shifted to $T=T_S$ (provided that $T_S>T_{w0}$). This prediction can be understood by means of diagrams similar to Fig. 25.

Using naive VW calculations, one expects the Hamaker

[6]This was pointed out to me by M. Schick.

constant A to be a quadratic function of the polarizabilities α_i,

$$A \sim (\alpha_S - \alpha_L)(\alpha_L - \alpha_V) ,$$

and the switching temperature T_S corresponds to

$$\alpha_L(T_S) = \alpha_S .$$

Thus there will exist a second-order wetting transition at $T = T_S$ provided that a number of conditions are satisfied:

(1) The "bare" transition T_{w0} is of second order.

(2) There exists a T_S: the polarizability of the dense liquid must be higher than α_S, while the liquid polarizability at the critical point must be smaller than α_S.

(3) T_S is above T_{w0}.

(4) Although the preceding discussion involved only the leading term in the long-range potentials [$V(\zeta) \sim \zeta^{-2}$], we must make sure that at the temperature T_S, where this leading term vanishes, the next term ($\sim \zeta^{-3}$) does not upset the order of the transition. This has been analyzed (Dietrich and Schick, 1984; Ebner, Saam, and Sen, 1984; Kroll and Meister, 1984), and imposes another condition.

From an experimental point of view, the conditions (1)—(4) are not easy to satisfy simultaneously. But there remains some hope of finding a second-order transition by an intelligent tuning of parameters.

b. Limitations and improvements

The discussion on the effects of long-range forces based on Fig. 25 has the merit of being simple, and has been used by a number of authors (Pandit *et al.*, 1982; Hauge and Schick, 1983; Tarazona and Evans, 1983; Tarazona, Telo da Gama, and Evans, 1983; de Gennes, 1983; Teletzke *et al.*, 1983; Privman, 1984). The discussion, however, has certain limitations which should be kept in mind. (See the review by Sullivan and Telo da Gama, 1985.)

(1) It holds only when the L/V interface thickness ξ is not too large, so that the film has a well defined thickness ($\zeta \gg \xi$). Thus the close vicinity of the L/V critical point would require a special study.

(2) Fluctuations of the L/V interface could modify the effective film energy in a profound way. This possibility was mentioned in particular by Pandit *et al.* (1982), and was studied in detail by Nightingale *et al.* (1983), using a "solid on solid" model, but in a temperature regime (above roughening) that made it adequate for the L/V interface. They did not find any dramatic effects of the fluctuations. We can understand this as follows:[7] the fluctuating interface is restricted in its motions by the presence of the solid wall. This entropy reduction creates an effective potential $V_f(\zeta)$ (where f stands for fluctuation), and $V_f(\zeta)$ is a rapidly decreasing function of ζ. In the absence of long-range forces, $V_f(\zeta)$ is an essential component of the theory for second-order transitions. But in the presence of long-range forces, which decay much more slowly with distance than $V_f(\zeta)$, fluctuation effects become negligible. Thus, even if one finds a second-order transition at some $T = T_S$, as explained above, this transition is expected to be of the mean-field type.

(3) It is incorrect to assume exponential tails for the L/V interface [Eq. (3.11)] when the interactions between molecules in the fluid become long range. The $(\nabla\rho)^2$ expansion of Eq. (3.2) then becomes invalid. This was noticed long ago by Christiansen (see Plesner and Platz, 1968) and more recently by de Gennes (1981) and Rowlinson, Barker, and Henderson (1981). What happens when the $(\nabla\rho)^2$ expansion breaks down? A first attempt to answer this question is due to Sullivan (1979,1981). He chose a pair interaction,

$$U(r_{ij}) = -\frac{\alpha}{4\pi r_{ij}} e^{-\gamma_1 r_{ij}} , \tag{3.17}$$

and a solid/molecule interaction with the *same* range γ_1^{-1},

$$V(z_i) = -\varepsilon_w e^{-\gamma_1 z_i} . \tag{3.18}$$

Sullivan showed that this special choice allows for a simple solution of the complete (integral) mean-field equations for $\rho(z)$, without assuming a $(\nabla\rho)^2$ expansion. He reached some interesting physicochemical conclusions. High ε_w led to plots where $\theta_e(T)$ was decreasing (as it is in the Cahn theory), while low ε_w led to θ_e increasing with T. His wetting transitions were of second order, but later work of Teletzke *et al.* (1983) and Benner *et al.* (1984), with the same model, ultimately led to first-order transitions. (The more complex situation with different γ_1 parameters in U and V was studied by Hauge and Schick, 1983.) In any case, the exponential interactions (3.17) and (3.18) are not adequate to study the order of the transition. They lead to a film energy $\rho(z)$ which is also exponential, and thus more abruptly decreasing than the expected VW term ($\sim \zeta^{-2}$).

It is more instructive to keep realistic VW interactions; this was done in numerical calculations by Tarazona and Evans (1983). Using the standard 6-12 potential, they found wetting transitions that were constantly of first order. This, in our view, does not mean that second-order transitions are entirely ruled out. But the conditions for a second-order transition in the presence of long-range forces, as deduced from the analysis of Dietrich and Schick (1984), are so stringent that they were not met in any of the cases considered in recent numerical calculations.

Tarazona *et al.* (1983) also extended these calculations and considered the equilibrium thickness of wetting films. Their results agree with the macroscopic predictions of Fig. 25.

An interesting extension of these ideas has been worked out very recently by Evans and Tarazona (1984). Instead of a single plate, exposed to a liquid or a gas, they consid-

[7] I am indebted to M. Schick for this presentation.

er *two parallel plates,* separated by a gap of width H_g. Using the Sullivan trick, they compute the effective interfacial energies $2\gamma_{SL}(T,H_g)$ and $2\gamma_{SV}(T,H_g)$ as a function of H_g. For a given H_g there may exist a transition temperature $T_c(H_g)$ such that, at this temperature, $\gamma_{SL}=\gamma_{SV}$. For large H_g this T_c coincides with the wetting transition point T_w. For small H_g, they find that the transition line $T_c(H_g)$ ends up at a critical point (this, however, occurs when H_g is comparable to the range of the forces, and may thus be rather sensitive to detailed local effects).

c. Prewetting transitions

Our discussion in this section was restricted to cases of macroscopic coexistence between liquid and vapor. If we impose a vapor pressure p_v *below* the value $p_{eq}(T)$ for liquid/vapor equilibrium, we cannot maintain a macroscopic L phase, but we may still have a film of L near the solid. The equilibrium thickness of these films can be analyzed in terms of a graph very similar to Fig. 24: we need only add a term linear in ζ (with a slope proportional to the difference in chemical potential between vapor and liquid). In many cases one still finds competition between two minima, and a possible first-order transition between them—describing a switch from a thick film to a thin film. For more details on this "prewetting transition" the reader is referred to Ebner and Saam (1977), Tarazona and Evans (1983), and Nakanishi and Fisher (1982).

6. Impurity effects: facts and conjectures

a. Facts

We have already mentioned in Sec. III.A that chemical contaminants may have dramatic effects on the wetting behavior of a liquid/liquid system. This was recognized from direct observations of contact angles (Moldover and Cahn, 1980) and substantiated by various measurements on the cyclohexane/methanol system near the free surface S. The contaminant was either water (Beaglehole, 1983; Tverkrem and Jacobs, 1983) or acetone (Cohn and Jacobs, 1983)—but in the latter case water may also have been present as a second contaminant. The Beaglehole experiments on water effects were based on ellipsometry. They are summarized below in terms of three different regimes, for a sample with 0.3% water.

(i) Very close to the critical point ($T_{on}<T<T_c$) no significant wetting film is observed.

(ii) In a certain temperature range ($T_{off}<T<T_{on}$) a wetting film of the β phase (methanol rich, heavy) is observed. The unfavorable gravitational potential of the β phase is compensated by the attractive force between S and methanol. Beaglehole also mentions *fluctuations* of the thickness (near T_{on}) plus a long time *drift* of the thickness (in most of the temperature interval).

(iii) At lower temperatures $T<T_{off}$ only a very thin residual film remains and methanol partially wets the free surface.

A very remarkable feature of these experiments is that, in the absence of water, the two transitions disappear: there is no detectable wetting film (at the free surface) at any $T<T_c$ for the pure system.

b. Tentative interpretations

(i) Surface transitions. One line of thought, advocated by Leibler (1984), is based on a possible similarity between surface transitions and the effect of He_3 impurities in superfluid He_4. Near a solid surface He_3 is depleted (less attracted than He_4) and superfluidity is favored. The result is the existence, in a small temperature range, of a two-dimensional superfluid phase near the solid, while the bulk He_4+He_3 system is still normal. Similar surface transitions—induced by water impurities—could occur in the cyclohexane/methanol system, and be responsible for anomalous behavior in a small region near T_{c0}. But it is not easy to interpret in these terms the lack of any observable film in region (i).

(ii) Macroscopic balance of interfacial tensions. The idea here is to describe the competition of water and methanol for the free surface, making use only of the macroscopic surface tensions γ_{ij} between the various partners (S, α, β, and $W\equiv$water). Let us assume the following structure for the γ_{ij}:

$$\begin{aligned}&\gamma_{sw}\sim\text{independent of } T\ ,\\ &\gamma_{s\alpha}=\gamma_{sl}-m\gamma_s'\ ,\\ &\gamma_{s\beta}=\gamma_{sl}+m\gamma_s'\ .\end{aligned}\tag{3.19}$$

Here γ_{sl} is the surface tension of the critical mixture. Following Cahn (1977) it is assumed that $\gamma_{s\alpha}-\gamma_{s\beta}$ is proportional to the difference in concentration between α and β, the latter being itself proportional to $m=(\Delta T/T_c)^{1/3}$. The coefficient γ_s' is postulated to be *positive.* This means that, in the absence of water, the free surface prefers the α phase. Since this is also the lighter phase, it will occupy a macroscopic region below the free surface, and no wetting film is expected (in agreement with the observations on water-free systems).

Let us now list the other interfacial tensions:

$$\gamma_{\alpha\beta}\equiv\gamma\sim\frac{kT}{\xi^2}\sim\gamma_1 m^4\tag{3.20}$$

(where we have used a classical scaling ansatz and the approximation $\beta=\frac{1}{3},\nu=\frac{2}{3}$ for the standard critical exponents)

$$\begin{aligned}&\gamma_{w\alpha}=\gamma_{wl}+\gamma_w' m\ ,\\ &\gamma_{w\beta}=\gamma_{wl}-\gamma_w' m\ .\end{aligned}\tag{3.21}$$

We expect γ_w' to be strongly positive (the water/methanol interfacial tension being much smaller than the water/hydrocarbon tension).

Having defined the surface tensions, we may now construct the spreading coefficients S, defined as in Sec. II. Here we shall call S_{ijk} the spreading coefficient for a film of (j) being spread between phase (i) and phase (k),

$$S_{ijk}=\gamma_{ik}-(\gamma_{ij}+\gamma_{jk}) . \tag{3.22}$$

As we know from Sec. II, a positive S means spontaneous spreading and buildup of a wetting film. The first spreading coefficient of interest is

$$\begin{aligned} S_{sw\beta}(T)&=\gamma_{sl}-\gamma_{sw}-\gamma_{wl}+m(\gamma'_s+\gamma'_w) \\ &=S_{sw\beta}(T_c)+m(\gamma'_s+\gamma'_w) . \end{aligned} \tag{3.23}$$

Let us assume that $S_{sw\beta}(T_c)<0$, so that, at the critical point, water does not wet the $S\beta$ interface. However, when we decrease T (increase m), because the coefficient $(\gamma'_s+\gamma'_w)$ is expected to be strongly positive, we may rapidly reach a temperature T_{on} such that

$$S_{sw\beta}(T_{on})=0 . \tag{3.24}$$

Below this temperature we do have a water film, and we must now consider the possible spreading of the β phase between water and α. Making use of the definition (3.22) and of the listed γ_{ij} values, we arrive at

$$S_{w\beta\alpha}=2m\gamma'_w-\gamma_1 m^4 , \tag{3.25}$$

and when m increases (T decreases) we may switch from positive $S_{w\beta\alpha}$ (wetting film of β) to negative $S_{w\beta\alpha}$. Thus we expect a second transition at $T=T_{off}$, where

$$S_{w\beta\alpha}(T_{off})=0 . \tag{3.26}$$

At this point, the system becomes unable to sustain a sequence gas|water|β|α. It may then achieve one of the following conformations:

$$\text{gas}\,|\,\text{water}\,|\,\alpha \quad \text{if} \quad S_{sw\alpha}>0 ,$$

$$\text{gas}\,|\,\alpha \quad \text{if} \quad S_{sw\alpha}<0 .$$

The formula for $S_{sw\alpha}$ is obtained from (3.23) by interchanging m and $-m$,

$$S_{sw\alpha}=S_{sw\beta}(T_c)-m(\gamma'_s+\gamma'_w) . \tag{3.27}$$

With our assumption, all terms in (3.27) are negative. We thus expect the water film to redissolve when we cool down below T_{off}, and the α phase to be in direct contact with the surface, leaving only a very thin layer (ξ) of excess cyclohexane. This scenario thus appears compatible with the data. Clearly this model is tentative and very rough. The water film may be much too thin to justify these purely macroscopic arguments, and it may be that there is no sharp W/α interface (if water is entirely soluble in α).[8] But the trend is interesting. The slow drift, and the fluctuations, seen in the interval $T_{off}<T<T_{on}$, could be due to the slow buildup of water content at the surface by diffusion and random convection.

[8]I am indebted to G. Teletzke for this remark.

It may be worthwhile to mention at this point another strange system, studied by Ross and Kornbrekke (1984). This is cyclohexane/anilin against glass. Here, at low temperatures, $\cos\theta$ is an increasing function of T, and reaches unity at a special temperature T_1. But above T_1, $\cos\theta$ *decreases* smoothly. It may be that this reflects a very fundamental multicritical behavior. But it may also be an impurity effect. When we reach $T=T_1$, an anilin film spreads over the capillary wall and may trap an impurity (water?) from distant sources. Then, at $T>T_1$, we would be dealing with a different surface (glass wet by impurity).

Clearly, all the binary mixtures under discussion (hydrocarbon/polar liquid) have chemical difficulties, such as trapping of water or spontaneous decomposition, and these difficulties are enhanced when the surface S is glass, which is also amenable to ion exchange, etc. Full control of impurity effects will require long, patient experiments.

(iii) Effects of long-range forces. The above interpretation assumed that long-range forces do not play a major role in the *existence* of the films, although they clearly control the *thickness* of a film.

An opposite viewpoint has been taken by Law (1984). Further, using a certain (assumed) form for the VW energies of films when the thickness (ζ) is not very large compared to the width of the α/β interface, he attempts to discuss the near vicinity of the bulk critical point (domain of large ξ). He finds three roots for the equilibrium film thickness, and claims that, in a certain range, all three roots are locally stable. The competition between three states then gives interesting possibilities, but it is hard to see how an energy function could have three distinct minima without having two intermediate maxima, also showing up as roots; thus this calculation is open to some doubt.

Another line of thought has been suggested by Israelashvili (1984). He pointed out that in certain layer systems (with dipoles present) the retarded/nonretarded VW energies may be of opposite signs (in a certain temperature range). This could lead to new energy minima, or maxima, in Fig. 6, and lead to our phase transitions.

IV. THE DYNAMICS OF SPREADING

A. Macroscopic measurements

Many practical problems involve a liquid spreading on a solid and displacing a gas. However, long, patient efforts have been required to obtain quantitative data on these problems. First, one must eliminate hysteresis effects. As we have seen in Sec. II, this is not a dream. With a reasonably (but not perfectly) smooth and homogeneous surface, no hysteresis should be left. Second, one should choose a simple flow geometry—eliminating, for instance, gravitational effects (which are often important in practice, but not very fundamental). A loose, but useful, condition for getting rid of gravitation is that the

linear dimensions of the drop (or of the meniscus) studied be small when compared to the capillary length $\kappa^{-1}=(\rho g/\gamma)^{1/2}$. Similarly, with common viscous fluids, one wishes to eliminate all inertial effects. We shall restrict our attention to slow, viscous flows, except in one section, which will be devoted to the opposite case of superfluid helium 4, where inertia is dominant.

A general review on the significance of the experiments has been given by Dussan (1979). Two arrangements, which satisfy the above requirements, have been used in detailed experiments: forced flow in a capillary and spontaneous spreading of a drop on a horizontal solid.

The choice of materials has not been very systematic. The liquids, in particular, are often selected because they have a viscosity that falls in a convenient range, one typical example being silicone oils. In fact, these oils are polymer melts, which may have very anomalous flow fields in the vicinity of the solid; fortunately, however, as we shall see in the theoretical sections, there are reasons to believe that the macroscopic laws are weakly (logarithmically) sensitive to these special properties. Thus the experiments described below are probably meaningful, even when they make use of these oils.

Most experiments have been performed with fluids that wet the solid completely, but there remains a fundamental ambiguity, because this may correspond either to $S=0$ or to $S>0$. The case $S=0$ is expected to be exceptional for dry solids, but possible for moist solids ($\theta_e=0$). However, we know, from the static discussion of Sec. II, that in the moist case the thickness of the preexisting liquid film is not fixed, but depends on a control parameter. In complete L/V equilibrium, this is the height of the plate above the reservoir providing the equilibrium.

At present, we do not seem to have any data from experiments on spreading, in the moist case, with prescribed values of this control parameter. Most existing experiments refer to the dry case, and probably correspond to $S>0$. But clearly the role of initial conditions should be considered more precisely in future work.

1. Forced flow in a capillary

The geometry chosen by Hoffman (1975) is shown in Fig. 26. He used a glass capillary (with a diameter ~ 2 mm), inside which a fluid was forced with velocities varying over five decades. The dimensionless parameter

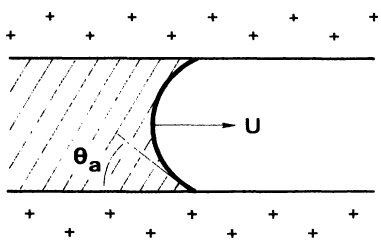

FIG. 26. Principle of the Hoffman experiments.

$$w=\frac{U\eta}{\gamma}=\frac{U}{V^*} \quad \text{(capillary number)} \tag{4.1}$$

(where η is the fluid viscosity) ranged between 10^{-4} and 10. Hoffman measured an *apparent contact angle* θ_a by a photographic technique. In a first series of experiments with silicone oils, he obtained conditions of complete wetting ($S\geq 0$) and found a rather universal relation between θ_a and w (Fig. 27):

$$w=F(\theta_a)\ . \tag{4.2}$$

Of particular interest is the low velocity limit ($w\to 0$), where the Hoffman data can be represented in the form

$$w=\text{const}\times\theta_a^m \tag{4.3}$$

with $m=3\pm 0.5$. Thus $\theta_a(w)$ first increases like $w^{1/3}$, and ultimately saturates at $w=1$, $\theta_a\to\pi$.

In a second series of experiments, Hoffman worked with other oils and industrial products, giving partial wetting ($\theta_e\neq 0$). He then found that his data could still be expressed in terms of the same F function, by writing

$$w=F(\theta_a)-F(\theta_e)\ . \tag{4.4}$$

However, the result (4.4) is much less documented than the data for complete wetting, and is open to some doubt.

These experiments clearly suffer from some defects. The materials were chosen mainly for their industrial interest, and many of them could carry contaminants. Ten years later, we are still lacking systematic data on pure (nonpolymeric) liquids, as well as on polymers of controlled molecular weight. It would be also be of interest to find out whether the apparent contact angle, as measured in photographs, at a given U, is independent of the capillary diameter. [Recent studies by Dussan and Ngan (1982) indicate that there is in fact some dependence.]

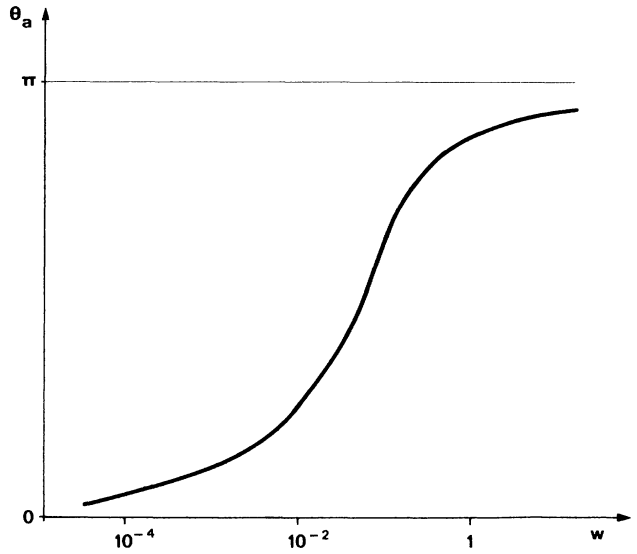

FIG. 27. Relation between reduced velocity $w=U\eta/\gamma$ and apparent contact angle θ_a (silicone oils on glass), after Hoffman (1975). At low w the relation is close to $\theta\sim w^{1/3}$.

However, in spite of these limitations, it is clear that the Hoffman experiments represent an important advance. The universal law (4.2) is very important. In particular, it is amazing to see that it holds without alteration for liquids of different S ($S>0$): *the magnitude of the spreading parameter has no influence.* We shall explain this in detail later.

2. Spreading of a droplet

Here most experiments have been performed for complete wetting ($S\geq 0$). The principle is shown in Fig. 28. In the classical approach, the expanding radius $R(t)$ is measured from photographs. In other studies, the nearly flat droplet is used as a lens. From the focal length of this lens one can go back to the apparent contact angle $\theta_a(t)$.

In the regimes where gravitation is negligible, the macroscopic shape of the droplet is found to be rather close to a spherical cap. Then the apparent contact angle, the drop thickness $h(t)$, and the radius $R(t)$ are related by

$$h=\tfrac{1}{2}R\theta_a\ , \tag{4.5}$$

$$\frac{\pi}{2}hR^2=\Omega\ , \tag{4.6}$$

valid for thin droplets ($\theta_a\ll 1$), this being the most important regime for complete spreading. Here Ω is the droplet volume and is assumed to be constant (weak evaporation).

Experimentally it is found that $R(t)$ increases rapidly at the early stages, and then very slowly. The data can often be represented (in terms of the wetted area πR^2) by a power law:

$$\pi R^2(t)\cong t^n\Omega^p\ . \tag{4.7}$$

The values of n obtained by different groups on different systems have been compared in a review by Marmur (1983). For water on glass, the early data of Hyppia (1948) suggest $n=0.22$, but Lelah and Marmur (1981) have found a strong temperature effect, with n ranging from 0.16 at 29 °C to 0.32 at 15 °C. One of the most accurate studies was performed by Tanner (1979) on silicone oils, and gave $n=0.21$. The exponent p has not been studied with the same detail, but is of order $\frac{2}{3}$ in the experiments of Lelah and Marmur (1981).

Some general remarks on the exponents n and p are in order at this point. Let us assume that the relation between apparent contact angle and velocity is correctly described by Eq. (4.3) and that the relevant velocity is the velocity of the contact line,

$$U=\frac{dR}{dt}\cong\frac{\gamma}{\eta}\theta_a^m\cong V^*\theta_a^m\ . \tag{4.8}$$

If we make use of the spherical cap approximation [Eqs. (4.5) and (4.6)] to eliminate θ_a, we arrive at

$$\frac{dR}{dt}\cong V^*\left[\frac{\Omega}{R^3}\right]^m\ , \tag{4.9}$$

and the spreading law becomes

$$R^{3m+1}\cong V^*t\Omega^m\ . \tag{4.10}$$

Thus we expect

$$n=\frac{2}{3m+1}\ , \tag{4.11}$$

$$p=\frac{2m}{3m+1}\ . \tag{4.12}$$

Taking the most probable value $m=3$ from the Hoffman data, we are then led to $n=0.20$ and $p=0.60$. We shall see below that $m=3$ is indeed expected theoretically for all cases of dry spreading ($S>0$).

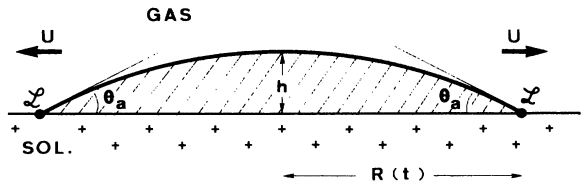

FIG. 28. A nearly flat droplet spreading on a solid: the macroscopic picture.

B. The precursor film

In the course of his pioneering work on wettability, Hardy (1919) recognized that a spreading droplet is announced by a precursor film (of submicrometer thickness), which shows up ahead of the nominal contact line. In particular, for droplets spreading on a solid surface, the film was revealed through its lubricating effects: a small test particle can slip more easily on the solid when the precursor is present. Hardy believed that these films occurred only with volatile liquids, which could condense ahead of the advancing droplet. This process may well exist, but more recent examples suggest that the film is present even in the absence of any vapor fraction (Bangham and Saweris, 1938; Chang *et al.*, 1982).

Detailed optical studies were carried out on the film at the Naval Research Laboratory (Bascom *et al.*, 1964), using nonpolar liquids which give complete spreading on steel. They found a precursor film, visible in ellipsometry at the late stages of spreading, with thicknesses of a few hundred angstroms. They also found (with impure liquids) a thicker, secondary film, probably due to Marangoni effects—a volatile contaminant being eliminated near the front and creating gradients of γ. We return to this impurity effect in Sec. IV.F.2, but omit it from the present discussion.

In one case, with a molten, viscous glass (which can be quenched and examined later), the film obtained by spreading on a metal was seen by electron microscopy (Radigan *et al.*, 1974). But the most brilliant detection of the film was based on electrical resistance measurements (Ghiradella *et al.*, 1975). The setup is slightly more complex [Fig. 29(a)], with a vertical plate and a conducting

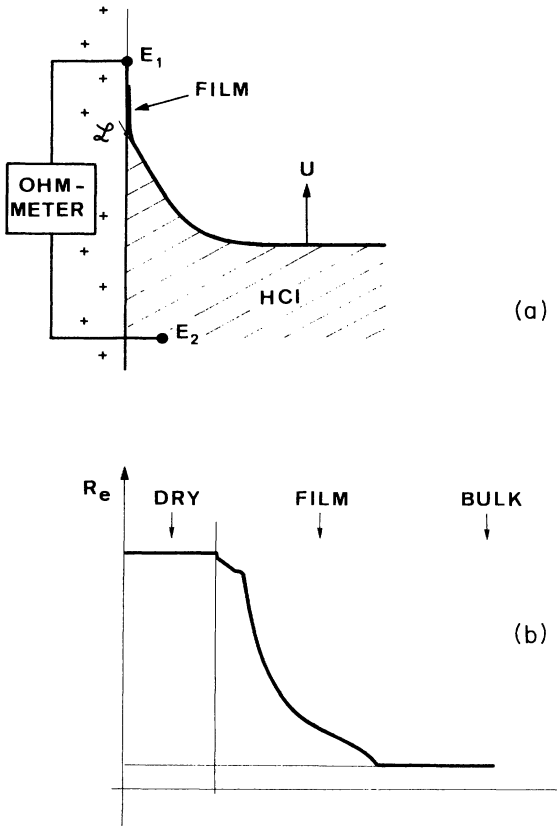

FIG. 29. Electrical detection of the precursor film (Ghiradella *et al.*, 1975). (a) Principle: the resistance $R_e(t)$ between two electrodes E_1E_2 is measured. (b) Typical record of $R_e(t)$: as soon as the film reaches (E_1), $R_e(t)$ drops.

liquid HCl that is set in vertical motion (velocity U). One measures the conductance between the bulk of the liquid (E_2) and an electrode (E_1) attached to the solid, when the nominal contact line $\mathscr{L}$ has not yet reached the electrode E_1. One finds a finite conductance occurring well in advance (e.g., when E_1 is one millimeter ahead of $\mathscr{L}$). A typical decrease of resistance with time is shown in Fig. 29(b). In principle, this could be translated into a profile $\zeta(x)$.

In practice, however, all the experiments we have described suffer from serious limitations: impurity effects resulting in gradients of the surface tension γ; choice of liquids, the polymer systems being in fact quite special, as explained in Secs. IV.B and IV.D; use of transient regimes (in the electrical experiments, where the velocity is imposed suddenly); noise and instability effects.

For all these reasons, we do not yet have a quantitative experimental law for the simplest (steady-state) film profile. But the situation should improve soon.

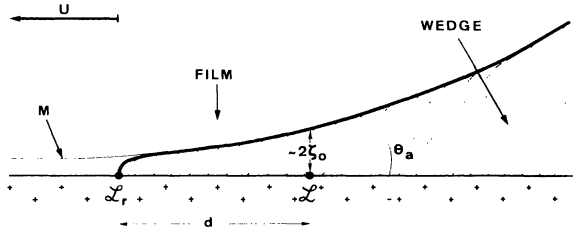

FIG. 30. A nearly flat droplet spreading on a solid: the microscopic picture.

C. Interpretation

1. Three types of dissipation

Let us restrict our attention to dry spreading ($S \geq 0$) of a pure, nonpolar liquid, attracted towards the solid by long-range van der Waals forces. Then the structure of the advancing front (with velocity U) corresponds to Fig. 30.

All macroscopic observations show the existence of a certain apparent contact angle θ_a. At distances $x \sim 100$ μm from the nominal contact line the fluid profile is very close to a *simple wedge* advancing along the solid. The motion of the liquid in this region has been probed in a clever experiment by Dussan and Davis (1974), marking the upper surface of the wedge with small spots of a dye (Fig. 31), and watching their motion (the liquid being highly viscous and the motion slow). They found a very characteristic rolling motion, reminiscent of a caterpillar

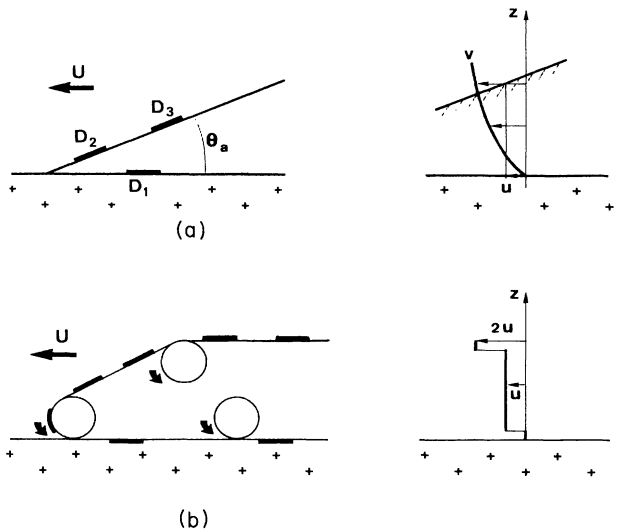

FIG. 31. (a) The Dussan-Davis experiment: spots of a dye $D_1D_2D_3$ are laid on the free surface of an advancing wedge. The spots slide down the wedge, and then get stuck to the solid. (b) The motion of a caterpillar vehicle is somewhat similar to the motion in the wedge [compare the velocity profiles $v(z)$].

vehicle. This rolling motion gives rise to viscous friction. We shall call the corresponding dissipation (per unit length of the contact line $\mathscr{L}$) $T\mathring{\Sigma}_w$, where the index w stands for "wedge."

Ahead of the wedge we have a *precursor* film (of typical thickness 100 Å) extending over a finite distance d. It has recently been realized (Hervet and de Gennes, 1984) that the viscous dissipation in this film is *very strong*. We shall call it $T\mathring{\Sigma}_f$.

The precursor film ends up by a *real contact line* $\mathscr{L}_r$ (shifted by a distance d from the nominal contact line $\mathscr{L}$). In the close vicinity of $\mathscr{L}_r$ we may have special losses, due to the attachment of liquid molecules to the solid. Some of the available free energy S may be transformed directly into heat. This third contribution is largely unknown; we shall call it $T\mathring{\Sigma}_l$ (where l stands for "local").

We can relate the total dissipation to the *unbalanced Young force* F, obtained by macroscopic considerations similar to Fig. 2:

$$F=\gamma_{SO}-\gamma_{SL}-\gamma\cos\theta_a \tag{4.13}$$

$$\cong S+\tfrac{1}{2}\gamma\theta_a^2 \quad (\theta_a \ll 1)\ . \tag{4.14}$$

Then the total dissipation is

$$FU=T(\mathring{\Sigma}_w+\mathring{\Sigma}_f+\mathring{\Sigma}_l)\ . \tag{4.15}$$

The common trend of the literature has been (i) to ignore $\mathring{\Sigma}_l$: we shall see that this may be correct in some favorable cases, and (ii) to ignore $\mathring{\Sigma}_f$: we shall see that this is grossly incorrect, and that, in fact,

$$T\mathring{\Sigma}_f=SU\ . \tag{4.16}$$

The free energy S is entirely burned in the film region.

2. Viscous losses in rolling motion

The flow patterns in a simple "wedge," advancing with constant velocity and angle θ_a [Fig. 31(a)], have been analyzed in a fundamental paper by Huh and Scriven (1971). They considered a very general case (arbitrary θ_a, nonzero viscosity in the gas phase). Here we shall present only a simplified view, holding for small θ_a and for negligible friction in the gas phase. This allows us to use the celebrated "lubrication approximation" of fluid mechanics. The idea is to treat the wedge as a nearly flat film, with a velocity profile

$$u_x(z)=u(z)$$

of the Poiseuille type [Fig. 31(a)]. On the solid side, u vanishes and on the gas side dw/dz vanishes (no tangential stress). The velocity U of the contact line is the z average of this profile,

$$U=\zeta^{-1}\int_0^{\zeta} dz\, u(z)\ . \tag{4.17}$$

(This may be checked by going to a frame moving with the line, where the solid slips at velocity $-U$, and where we find a steady state with 0 horizontal current.) One can then write

$$u(z)=\frac{3U}{2\zeta^2}(-z^2+2\zeta z)\ . \tag{4.18}$$

The viscous dissipation integrated over the film depth is

$$\int_0^{\zeta} dz\,\eta\left[\frac{du}{dz}\right]^2=\frac{3\eta U^2}{\zeta} \tag{4.19}$$

(where η is the fluid viscosity), and the total dissipation in the wedge is

$$T\mathring{\Sigma}_w=\int_{x_{\min}}^{x_{\max}}\frac{3\eta U^2}{\zeta}d\,|x|=\frac{3\eta U^2}{\theta_a}\ln\left|\frac{x_{\max}}{x_{\min}}\right|\ . \tag{4.20}$$

We expect $x_{\max}$ to be a cutoff related to the macroscopic size of the droplet $x_{\max}\sim R$. The cutoff $x_{\min}$ is more difficult to specify and will be discussed below. But without any cutoff ($x_{\min}\to 0$) the dissipation would diverge; as explained in Hellenic terms by Huh and Scriven (1971), "not even Herakles could sink a solid!"

Various physical processes may remove the singularity, and the choice of process depends very much on the choice of systems.

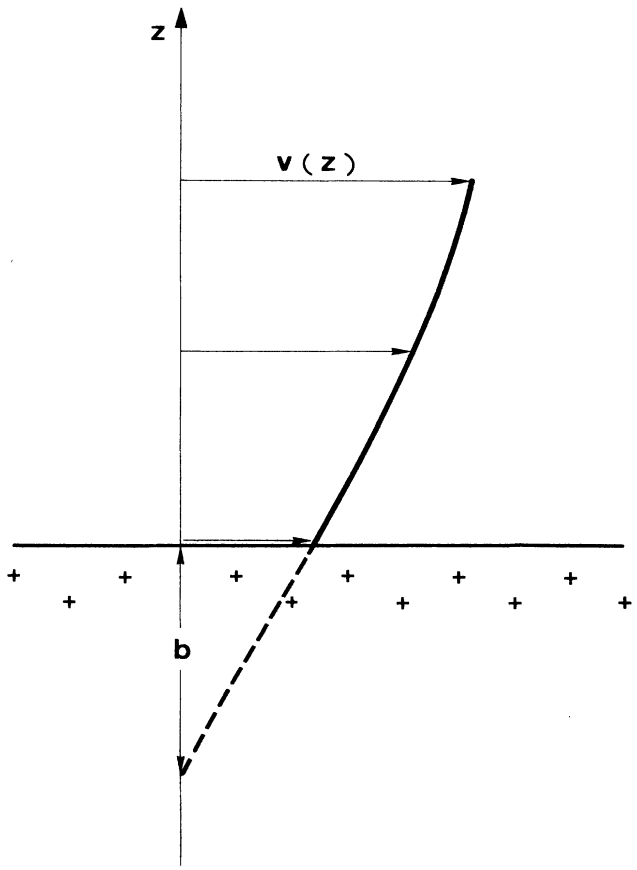

FIG. 32. The extrapolation length b characterizes the amount of slippage allowed in viscous flow near a solid surface.

a. Finite slippage at the solid surface

Instead of imposing zero velocity on the fluid (in the solid's frame) at the solid surface, it is natural to allow for a small amount of slippage, described by an extrapolation length b (Fig. 32). This may occur in various systems.

(i) A porous solid, saturated with the same fluid, will allow for an exponential tail in the velocity field. This could be found in nature—for instance, static contact angles have been studied on a "solid" made of a swollen silica gel (see Michaels and Dean, 1962)—but has not been studied systematically.

(ii) A rough solid surface may possibly be described along similar lines (Hocking, 1976). This, however, is not a very attractive situation, because roughness implies all the complications of hysteresis—discussed in Sec. II.C.

(iii) A normal liquid flowing over a smooth solid will display a length b comparable to the molecular size a. As we shall see, for this most important case, slippage is usually negligible, and the cutoff is provided by another effect (long-range VW forces).

(iv) Special physicochemical processes near the contact line have been proposed by Ruckenstein and Dunn (1976). They also lead to $b \sim a$.

(v) A polymer melt, flowing on a smooth surface (without any chemical attachment between polymer chains and the wall), is expected to show anomalously large values of b (de Gennes, 1979a). This generates special "foot structures" near the contact line, which are analyzed in Sec. IV.D.

A complete mechanical theory of macroscopic droplets spreading with finite slippage has been constructed by Huh and Mason (1977), and in more detail by Hocking (1977,1981) and Hocking and Rivers (1982). This theory is characterized by a matched asymptotic expansion between three regions—a "foot" where slippage dominates, a "wedge" with nearly constant slope, and a "central region" where the droplet is close to a spherical cap. This last feature deserves comment. In the thicker regions of the droplet, the flows are easy, and the mechanical pressure p_L equilibrates. The difference $p_L - p_V$ between the pressures in and out of the drop is constant, and this, in turn, through the Laplace-Young equation, means that the curvature of the L/V surface is constant, hence the spherical cap. The work of Hocking provides a precise proof of the above statement.

Quantitatively, as we shall see in Sec. IV.D, the result of slippage on the logarithmic cutoff $x_{\min}$ is simple: we expect

$$x_{\min} \cong b/\theta_a \ . \tag{4.21}$$

b. van der Waals forces

These lead to precursor films, and the film provides a cutoff for the dissipation $T\mathring{\Sigma}_w$. In cases of dry spreading with $S>0$, we shall see later that the cutoff is given by

$$x_{\min} \cong a/\theta_a^2 \ . \tag{4.22}$$

This dominates over slippage effects whenever the extrapolation length for slippage is comparable to the molecular size a [as can be seen by comparison of Eqs. (4.21) and (4.22)].

3. Structure and dissipation in the precursor film

The idea that a film can move because of a gradient of the disjoining pressure Π is not new (Deryagin, 1955; Lopez *et al.*, 1976; Starov, 1983). However, for the spreading of liquids on solids, progress, has been slow. A number of hydrodynamic flows have been solved numerically by Teletzke *et al.* (1983). The difficulty stems from the variety of experimental situations, revealed in the preceding paragraph. It is only by a patient separation of different physical regimes that one may hope to reach general laws (de Gennes, 1984a,1984b,1984c; Hervet and de Gennes, 1984).

Let us concentrate, then, on a "pure" case: a nonpolar liquid, giving complete wetting, and attracted towards the solid by VW forces. Transfer through the vapor is assumed to be negligible. There are no solute impurities, and we also exclude the case of polymers (the extrapolation length b for slippage is then negligible). Gravity effects are omitted. Finally, we restrict our attention to a *steady-state regime,* where the nominal contact line $\mathscr{L}$ moves with constant velocity $(-U)$ with respect to the solid (Fig. 31). We shall, in fact, work in the frame of the line, where the solid moves with a velocity $+U$. The choices of steady state, rather than transients, simplifies the equations enormously.

a. Hydrodynamic equations

Our starting point will be the pressure distribution in the film $p(x,z)$, which has the following structure:

$$p = p_G - \gamma \frac{d^2\zeta}{dx^2} + W(\zeta) - W(z) \ , \tag{4.23}$$

where p_G is the gas pressure; the second term represents the Young-Laplace capillary term. $W(\zeta)$ is the VW energy (per unit volume of liquid) between liquid and solid. In the nonretarded regime, which will be our main concern here, we have from Eq. (2.41)

$$W(z) = -\Pi(z) = -\frac{A}{6\pi z^3} \ . \tag{4.24}$$

Locally Eq. (4.23) describes a hydrostatic equilibrium. The vertical force acting on any volume element vanishes,

$$-\frac{\partial p}{\partial z} - \frac{\partial W}{\partial z} = 0 \ . \tag{4.25}$$

The term $W(\zeta)$ in (4.23) ensures that $p(\zeta)$ reduces to the Laplace-Young value.

In the lubrication approximation, the horizontal current J_S (in the frame of the solid) is given by a Poiseuille formula:

$$J_S=\frac{\zeta^3}{3\eta}\left[-\frac{\partial p}{\partial x}\right] . \tag{4.26}$$

In the frame of the line $\mathscr{L}$ this current becomes

$$J=U\zeta+J_S . \tag{4.27}$$

For steady-state solutions, J must be independent of x and t. In fact, for our problem (where there remains no film far ahead of the line $\mathscr{L}$), J must vanish exactly. This leads to the basic equation

$$\frac{3\eta U}{\zeta^2}=\frac{d}{dx}\left[-\gamma\frac{d^2\zeta}{dx^2}+W(\zeta)\right] . \tag{4.28}$$

Equation (4.28) describes not one, but many types of precursors, depending on the value of the spreading coefficient S. However, before discussing all these possibilities, it is instructive to return first to the macroscopic limit—i.e., to values of ζ that are large, so that $W(\zeta)$ becomes negligible. Then (4.28) reduces to an equation studied by Tanner (1979). We are particularly interested in solutions that have zero curvature for large ζ (i.e., that tend to behave nearly like a simple wedge in the macroscopic limit). They have the asymptotic form

$$\zeta(x)\rightarrow x\left[\frac{qU}{V^*}\ln\left[\frac{x}{x_1}\right]\right]^{1/3} , \tag{4.29}$$

and the slope varies very slowly with x. The constant x_1 will be determined later by matching Eq. (4.29) with appropriate solutions (at $x<0$) which describe a precursor film.

b. The "maximal" film

Let us consider first the profile marked M in Fig. 33. With this profile, we have a film that is present over *all* the solid surface. It will turn out that this "maximal" situation is relevant when the spreading coefficient S is positive and not too small ($S\gg\gamma\theta_a^2$). For the "maximal" case, there is no contact line $\mathscr{L}$, at the microscopic level, and the precursor is a nearly flat film. It is then permissible to drop the γ term in Eq. (4.28) over the whole film region ($x<0$).

Using (4.24) for $W(\zeta)$, and the definition (2.50) of the molecular length a, we can then reduce Eq. (4.28) to the simple form

$$\frac{a^2}{\zeta^2}\frac{d\zeta}{dx}=\frac{U}{V^*}\equiv w . \tag{4.30}$$

This can be integrated immediately to give the maximal film profile:

$$\zeta(x)=\frac{a^2}{w(x_2-x)} , \tag{4.31}$$

where x_2 is another integration constant, which we shall take to be equal to zero in what follows. We shall see that, in nearly all practical cases, Eq. (4.31) describes an important portion of the film, where the thickness is decreasing only slowly ($\zeta\sim|x|^{-1}$) with distance.

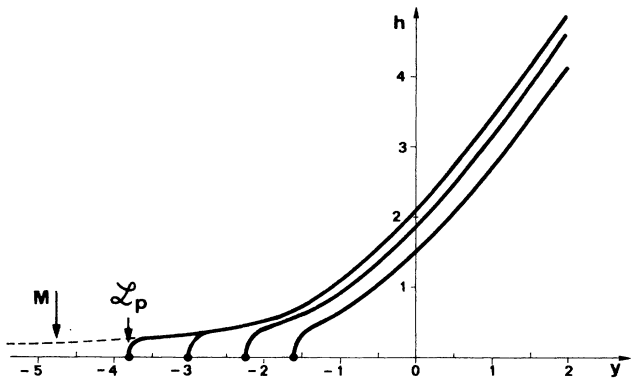

FIG. 33. A few numerical solutions of the film equation (4.33) for various values of the spreading parameter S (after Hervet and de Gennes, 1984). The larger S values correspond to the larger films.

c. Crossover between the maximal film and the macroscopic droplet

Let us first rescale (4.28) into an adimensional form,

$$\begin{aligned} &x=x_0y , \\ &\zeta=\zeta_0h(y) , \\ &x_0=3^{-1/6}aw^{-2/3} , \\ &\zeta_0=3^{1/6}aw^{-1/3} , \end{aligned} \tag{4.32}$$

$$h'h^{-2}-h'''h^2=1 , \tag{4.33}$$

where $h'\equiv dh/dy\cdots$. The "maximal" solution corresponds to $h(y\rightarrow-\infty)\rightarrow0$. There exists a one-parameter family of solutions of Eq. (4.33) which satisfies this condition, with the asymptotic form

$$h_\alpha(y\rightarrow-\infty)=-\frac{1}{y}+\alpha\exp(y^3/3) . \tag{4.34}$$

The $\alpha=0$ solution corresponds to Eq. (4.31). The other solutions ($\alpha\neq0$) are obtained by searching for small deviations from Eq. (4.31) and solving the corresponding linear equation in a WKBJ approximation. Starting from Eq. (4.34), one can extend the solutions $h_\alpha(y)$ towards positive y by numerical integration of Eq. (4.33) (Hervet and de Gennes, 1984).

One of these solutions ($\alpha=\bar{\alpha}\sim0.38$) has the limiting property

$$h_{\bar{\alpha}}''(y\rightarrow+\infty)=0 . \tag{4.35}$$

This is the solution of interest (because the curvatures on the macroscopic side are always very weak on the scale of the film). At large, positive y the solution $h_{\bar{\alpha}}(y)$ does reach the asymptotic form announced in Eq. (4.29),

$$h_{\bar{x}}(y) \to y f^{1/3}(y), \quad f(y) \equiv 3\ln(0.4y) . \tag{4.36}$$

Thus the cutoff length x_1 defined in Eq. (4.29) is

$$x_1 = 2.5 x_0 ,$$

where x_0 is defined in Eq. (4.32)

The most important observable is the *apparent contact angle* θ_a, defined by a measurement at a macroscopic distance x from the contact line $\mathscr{L}$ [$x_1 \ll x \ll R(t)$]. Using (4.34), we find

$$\theta_a \equiv \frac{d\zeta}{dx} = \frac{\zeta_0}{x_0} f^{1/3}(1+f^{-1}) \cong \frac{\zeta_0}{x_0} f^{1/3} , \tag{4.37}$$

and returning to Eq. (4.32) this gives the fundamental formula

$$\theta_a^3 = 3fw . \tag{4.38}$$

The main conclusions are the following.

(i) f is nearly constant, and $\theta_a \sim w^{1/3}$, as observed in the low-velocity experiments of Hoffman (1975) and Tanner (1979). An equation of this type was first derived theoretically by Fritz (1965), but for a slightly different problem (liquid spreading on a wet surface). It is probably fair to call Eq. (4.38) the *Tanner law*, because Tanner was the first to define it and to obtain it from experiments on a *dry* surface. He also interpreted his own experiments by similar ideas (although he did not take the precursor film into consideration). Of course, the exponent 3 in Eq. (4.38) is only approximate, because f is logarithmically dependent on w, but this is a minor refinement.

(ii) The width of the crossover region between film and droplet is of order $x_0 = aw^{-2/3}$ [Eq. (4.32)]. After making use of Eq. (4.38), this becomes

$$r_0 \cong a/\theta_a^2 . \tag{4.39}$$

(iii) The thickness of the film in the crossover region is

$$\zeta_0 \cong a/\theta_a . \tag{4.40}$$

Thus the precursor film has reality ($\zeta_0 \gg a$) only for situations of small θ_a. Typically $\theta_a = 10^{-2}$ and $a = 1$ Å, giving $\zeta_0 = 100$ Å (falling well into the range of nonretarded VW interactions).

d. Truncated films

We shall now show that the maximal film described above (covering the whole solid surface) corresponds to a certain limiting case of "dry" spreading, described by the inequality[9]

$$S \gg \tfrac{1}{2}\gamma\theta_a^2 . \tag{4.41}$$

This can be easily understood if we return to the static discussion of Sec. II.D. We saw there that a VW fluid with positive S does not spread on a dry solid down to a molecular layer, but in fact stops at a certain equilibrium thickness $e(S)$ [Eq. (2.72)],

$$e(S) \cong \left[\frac{\gamma}{S}\right]^{1/2} a . \tag{4.42}$$

It is natural to expect that the precursor film never thins down below this value. The maximal film solution is applicable only in the interval

$$e(S) < \zeta < \zeta_0 . \tag{4.43}$$

Setting $\zeta = e(S)$ in Eq. (4.31), we have a formula for the film width d:

$$d \cong \frac{a^2}{we(S)} \cong \frac{a}{w}\left[\frac{S}{\gamma}\right]^{1/2} . \tag{4.44}$$

These predictions are entirely confirmed by detailed numerical solutions of Eq. (4.33) (Hervet and de Gennes, 1984). The truncated solutions are shown in Fig. 33. They start at certain contact line $\mathscr{L}_r$ of position $x_r = -d$. The initial rise of the profile near x_r is parabolic and identical to the static solution [Eq. (2.55)]. At higher x the solution merges with the maximal profile, provided that $d \gg x_0$. The latter condition also shows up in Eq. (4.43). To have a film, we must satisfy

$$e(S) < \zeta_0 , \tag{4.45}$$

and this requirement is equivalent both to $d > x_0$ and to Eq. (4.41). In most practical cases we expect to have Eq. (4.41) well satisfied, in which case a film will indeed be present.

e. Dissipation in the film

A remarkable feature of the Tanner law (4.38) is that the value of the spreading coefficient S does not play any role (even in the log term). The only requirement is that the macroscopic profile cross over into a maximal film, and this, as we just saw, is satisfied whenever $S \gg \gamma\theta_a^2$. The Tanner law expresses a certain relation between the flux U and the force F in the thermodynamic formulation of Eq. (4.15). The spreading coefficient S is the dominant term in the force, so there is an apparent paradox. How does S drop out of the energy balance?

The viscous dissipation computed from the hydrodynamic equation (4.28) does agree with Eq. (4.15). The dissipation in an interval $-\infty < x < x_{\max}$ (where $x_{\max}$ is in the macroscopic region $x_{\max} \gg x_0$) is exactly

$$T(\mathring{\Sigma}_w + \mathring{\Sigma}_f) = \int_{-\infty}^{x_{\max}} \frac{3\eta U^2}{\zeta} dx . \tag{4.46}$$

Using the truncated solutions plus suitable integrations by parts (Hervet and de Gennes, 1984), we can transform this exactly into Eq. (4.15) (with the assumption $T\mathring{\Sigma}_l = 0$). Thus we have not forgotten anything in the energy balance. But where is the free energy S dissipated? We shall find the answer through a qualitative estimate of the

[9]This condition was not entirely appreciated in the original work (de Gennes, 1984a) on the maximal film.

losses in the film only,

$$T\mathring{\Sigma}_f=\int_{-d}^{0}\frac{3\eta U^2}{\zeta}dx\ , \tag{4.47}$$

where we use an abrupt truncation at $x=-d$ and also arbitrarily decide that the film stops exactly at $x=0$. We use the maximal film solution in this interval, in the form (4.30), and transform (4.47) into

$$T\mathring{\Sigma}_f=3\eta U^2a^2w^{-1}\int_{e(S)}^{\zeta_0}\frac{d\zeta}{\zeta^3}\ . \tag{4.48}$$

The leading term comes from the lower limit and is

$$T\mathring{\Sigma}_f=\frac{3\gamma a^2U}{2e^2(S)}=SU\ . \tag{4.49}$$

We now have the answer: all the excess free energy S is burned in the film. The remaining contribution to F, namely, $\frac{1}{2}\gamma\theta_a^2$, is used up in the wedge, and imposes the relation (4.38) between reduced velocity (w) and wedge angle θ_a, where S does not appear.

4. Spreading over a wet surface (Bretherton, 1961; Fritz, 1965; Tanner, 1979)

Let us return now to macroscopic droplets (or capillaries) and consider a solid that was initially covered with a liquid film of constant thickness (e_0). On top of this we add, for instance, a droplet, and watch its spreading.

a. Macroscopic regime

If e_0 is large ($e_0>1000$ Å) we may omit all effects of long-range forces, and we are dealing only with capillary energies that are dissipated by viscous flows. This family of problems was discussed long ago by Landau and Levich (1942; see Chap. 12 of the book by Levich, 1962). They were more concerned with a plate being pulled out of a liquid, while our present problem is the analog of a wet plate being pushed in, but the basic equations are the same. We may summarize the results by saying that the logarithmic cutoff discussed in Sec. IV.B.2 is now provided by the original film,

$$x_{\min}\cong e_0/\theta_a\ . \tag{4.50}$$

Inserting this into the wedge dissipation formula (4.20), we see that large $x_{\min}$ values correspond to a smaller logarithmic factor l, and should thus lead to larger velocities.

An interesting feature is that the profile is not monotonous: we expect small *capillary oscillations* ahead of the nominal contact line $\mathscr{L}$. Such an expectation arises from the linearized ($\zeta\to e_0$) steady-state equation, which is of third order and has exponential solutions with a complex decay length—leading to damped oscillations. These oscillations are, in fact, quite visible when moving a liquid in a prewetted test tube,[10] and are shown in photographs by Fritz (1965).

[10]I am indebted to Y. Pomeau for one of these observations.

b. Microscopic regime

If e_0 is smaller than the precursor characteristic thickness ζ_0 [Eq. (4.32)], the main effects should occur in the precursor region. Let us discuss them briefly, starting from the current in the frame of the line [Eq. (4.27)]

$$J=U\zeta-\frac{A}{6\pi\eta\zeta}\frac{d\zeta}{dx}\ , \tag{4.51}$$

where we have used Eqs. (4.23) and (4.24). In steady state J is constant, but the constant is now different from zero. In the far precursor region, the thickness $\zeta\to e_0$, and we must have

$$J=Ue_0\ . \tag{4.52}$$

This leads to a profile

$$\zeta(x)=\frac{e_0}{1-\exp(q\,|\,x-x_r\,|\,)}\ , \tag{4.53}$$

where x_2 is an integration constant, and

$$q=\frac{6\pi\eta e_0U}{A}\ . \tag{4.54}$$

The result (4.53) describes a crossover between the maximal precursor [Eq. (4.31)] found in the region $\zeta>e_0$ (or $q\,|\,x_2-x\,|\ll 1$) and an exponential tail,

$$\zeta(x)-e_0=e_0\exp(-q\,|\,x-x_2\,|\,)\ , \tag{4.55}$$

in the forward region ($\zeta-e_0\ll e_0$). We see that in the limit $e_0<\zeta_0$, the matching of the macroscopic solutions will be imposed by the conventional precursor, and the preexistant film of thickness e_0 should have only weak effects on macroscopic flows. More detailed numerical discussions of the various regimes have been carried out by Teletzke *et al.* (1983).

c. Spreading with obstacles

The ideas sketched in Secs. IV.A.4.a and IV.A.4.b above could be tested by relatively simple experiments using uniformly wet surfaces. But their main impact may be different. Some macroscopic experiments show that a moving contact line has a velocity sensitive to perturbations on the solid surface which lie *ahead of* $\mathscr{L}$.

(i) Bangham and Saweris (1938) noticed that a drop of methyl alcohol spreading on mica was slowed down when reaching the vicinity of a drop of butyl alcohol.

(ii) Lelah and Marmur (1981) showed that a water droplet spreading on a glass slide had its line $\mathscr{L}$ attracted towards the edge of the slide. This attraction was felt at distances ~ 1 mm.

All these situations are complex; one would like to know first what happens when two drops of the *same* liquid are spreading on a flat solid surface and on the verge of coalescing. Experimental studies on the macroscopic shapes would be easy to perform and (possibly) not too hard for theoretical analysis. Indeed, Teletzke, Davis, and Scriven (1984) have analyzed the Lelah-Marmur ex-

periment (ii). They can explain the sign of the effect if they assume for the disjoining pressure $\Pi(\zeta)$ of water on glass the slow decrease ($\Pi \sim \zeta^{-1}$) extracted from empirical data by Pashley (1980).

D. The special case of polymer melts

1. Observations

We are concerned here with flexible polymer chains, which can exist in a liquid form and give complete spreading ($S > 0$). To study these polymer drops is not very easy; one encounters at least two difficulties: high viscosities (if the chains are long) and impurity content (many practical polymer systems contain additives, or catalysts, from the fabrication process). This led to serious complications in the early experiments by Bascom *et al.* (1964).

However, the spreading of polymers such as silicone oils is important for many industries (paints, adhesives, protective coatings). Also, from a more fundamental point of view, we shall see that it raises a very special problem. Three main experiments indicate an anomalous behavior.

(a) Early work by Schonhorn *et al.* (1966) showed that a certain characteristic length (independent of the original size R_0 of the droplet) came into the spreading laws. Later work by the same group (Radigan *et al.*, 1974), using electron microscopy, displayed a "protruding foot" near the contact line $\mathscr{L}$.

(b) Ogarev *et al.* (1974) studied polydimethylsiloxane chains of high molecular weight ($M \sim 10^6$) spreading on mica. (They had only one value of M, but they could vary the viscosity significantly by changing the temperature.) Their main conclusion (from our point of view) was that the macroscopic shape of the drops is not a spherical cap, as it is with nonpolymeric, pure liquids. The deviation from sphericity is most significant for small droplet volumes. There is indeed a spherical cap region in the center, but the cap is surrounded by a protruding "foot" (Fig. 34). The foot is macroscopic and has nothing to do with the precursor of submicron thickness which was discussed in Sec. IV.C.

(c) Sawicki (1978) carried out a series of systematic spreading with silicone drops of different chain lengths. His results on the apparent contact angle $\theta_a(t)$ are not far from the Tanner law ($\theta_a \sim t^{-0.3}$). However, when he compared the bulk viscosity to the apparent viscosity η_a required to fit a wedge model, he found η_a values that were too low. His interpretation was that the macromolecules were elongated in the film region, and that this led to a reduction of viscosities. But this non-Newtonian behavior is open to doubt at the very low shear stresses achieved in spreading. An alternate explanation will be presented below.

2. Interpretation

The "protruding foot" has been a source of confusion in the past. To keep things straight, we must (i) carefully discriminate between the foot and the precursor film (as explained above), and (ii) put in a different class the special profiles observed by Bascom *et al.* (1964), which are associated with volatile impurities.

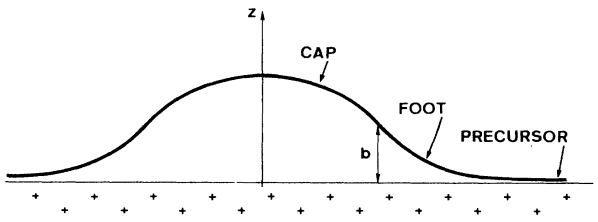

FIG. 34. Qualitative shape of a polymer melt during spreading.

a. Strong slippage

The basic idea, proposed independently of all spreading phenomena (de Gennes, 1979a), is that entangled polymers, flowing near a smooth, passive surface, should show a highly anomalous slippage, or, equivalently, a very large extrapolation length b (Fig. 32). Physically we may say that it is less expensive to concentrate the shear at the polymer/solid interface than to spread it over all the liquid (where entanglements oppose the shear very strongly). The resulting formula for b is

$$b = a\eta/\eta_0 , \tag{4.56}$$

where a is a molecular size, η_0 is the viscosity of a liquid of monomers (with the same interactions, but no entanglements), and η is the melt viscosity (enormously enhanced by the entanglements).

In the "reptation" model for molten polymers, one expects (de Gennes, 1979b)

$$\eta = \eta_0 \frac{N^3}{N_e^2} , \tag{4.57}$$

where N is the number of monomers per chain, while N_e is a characteristic number (the "number of monomers per entanglement"), of order 100. Experimental exponents are slightly higher than the value (3) predicted by (4.57), but the trend is clear: with high values of $N(10^4)$, one can expect to find b values up to one millimeter.

Early observations on the flow of polyethylene melts inside transparent capillaries give some support to these ideas (Galt and Maxwell, 1964). In these experiments, the velocity field was probed via tracer particles. It was found that the velocity at the well did *not* vanish in a significant fraction of the runs. Experiments by Kraynik and Schowalter (1981) detected the slip by hot film anemometry. Burton *et al.* (1983) used a Weissenberg rheogoniometer equipped with closely spaced parallel plates: for molten polystyrene ($M \sim 10^5$) the data indicate $b \sim 60$ μm. They are taken at relatively low shear rates: slippage does exist for Newtonian flows.

b. Droplet shapes
(Brochard and de Gennes, 1984)

Let us focus our attention on the most important case, where the droplet thickness at the center (h) is much larger than b, but b itself is macroscopic ($b > 1$ μm). One then expects to find three regions.

A spherical cap, where $\zeta \gg b$. Here normal viscous flow takes place, slippage is negligible, and the apparent contact angle θ_a should follow the Tanner law [Eq. (4.3)].

A macroscopic foot, where $b > \zeta > \zeta_0$. In this region we expect to find a "plug flow" of polymer driven by capillary forces.

A precursor film, where $\zeta_0 > \zeta$, which differs from the normal precursor of Sec. IV.C because the flow is again of the "plug" type.

Let us start with the macroscopic domain. For finite b, the equation for the horizontal current J_S, which replaces (4.26), is

$$J_S = \frac{\zeta^2}{\eta}(b + \zeta/3)\left[-\frac{\partial p}{\partial x}\right] . \tag{4.58}$$

If we work in a macroscopic regime, the only effect contributing to $\partial p/\partial x$ is capillarity,

$$-\frac{\partial p}{\partial x} \to \gamma \zeta''' , \tag{4.59}$$

and the steady-state equation becomes

$$w \equiv \frac{U}{V^*} = -(b + \zeta/3)\zeta\zeta''' . \tag{4.60}$$

At $\zeta \gg b$ we recover Tanner's equation, and the profile is a spherical cap. At $\zeta \ll b$, we can construct a special solution that describes the foot:

$$\zeta^2 = 8\,|x|^3/3\lambda , \tag{4.61}$$

$$\lambda = b/w . \tag{4.62}$$

Here $|x|$ is the horizontal distance measured from the nominal contact line $\mathscr{L}$. In principle, the crossover between the foot [Eq. (4.61)] and the spherical cap ($\zeta > b$) can be extracted from the work of Hocking (1977) and Hocking and Rivers (1982). For qualitative purposes, it is enough to note that the width f_1 of the foot must be such that Eq. (4.61), taken at $|x| = f_1$, gives $\zeta \sim b$. Thus

$$f_1 \cong (\lambda b^2)^{1/3} \cong b w^{-1/3} \cong b\theta_a^{-1} . \tag{4.63}$$

The logarithmic cutoff discussed in Sec. IV.B is now expected to be $x_{\min} \sim f_1$, as announced in Eq. (4.21).

c. The polymer precursor

If we now go to a microscopic regime, where VW forces become dominant, the equation for the maximal film is obtained by ignoring capillarity and setting

$$-\frac{\partial p}{\partial x} \to \frac{A}{2\pi\zeta^4}\frac{\partial \zeta}{\partial x} \tag{4.64}$$

(in the nonretarded regime). Inserting this into Eq. (4.58), choosing $\zeta \ll b$, and solving, one obtains

$$\zeta^2 = \frac{Ab}{4\pi\eta U}\frac{1}{|x - x_2|} , \tag{4.65}$$

where x_2 is an integration constant. Thus the thickness of the maximal precursor should decrease even more slowly than in conventional fluids ($\zeta \sim |x|^{-1/2}$). Note that the prefactor $\eta/b = \eta_0/a$ should be *independent of molecular weight* (for entangled systems). The scaling form of the crossover length x_2 is

$$x_2 \cong (ab)^{1/2}\theta_a^{-3/2} . \tag{4.66}$$

A truncation of the maximal precursor at finite S should occur as in Sec. IV.C.3, but has not yet been explored.

3. Perspectives

The existence of a macroscopic foot on spreading polymer droplets appears as a natural consequence of plug flows. It must be emphasized that the extrapolation length b, describing the plug flows, is very sensitive to the surface treatment (de Gennes, 1979a): if the surface is slightly rough, or if the surface can bind chemically to some of the chains (or to chain ends) b could be drastically reduced from the estimate (4.56). This means that a complete study of the spreading of polymer melts will require a delicate, coordinated effort between polymer science and surface science.

On the theoretical side, many aspects of polymer melts remain completely unexplored. The regimes at $h < b$ should not be ruled by the Tanner law, and may correspond to the observations of Schonhorn *et al.* (1966). Moreover, the discussion on surface friction, leading to Eq. (4.56) for b, has been carried out only in the limit of strongly entangled chains ($N \gg N_e$). With silicone oils of low N, which are of some practical interest, one needs an estimate of b in the opposite limit ($N < N_e$). We still expect an enhancement of b, and Eq. (4.56) may even remain qualitatively valid, but to prove this will require a delicate study of chain flow near a passive wall, which (fortunately) was not required in the entangled limit.

E. Spreading laws for superfluid He_4

A long experimental effort has been devoted to the statics of the Rollin film, and also to the small-amplitude oscillations of the film surface ("third sound"). Some studies have also been carried out on transport (from one reservoir to another, at a different level) via the film (see the review by Brewer, 1978). But we do not know of any observation on the horizontal spreading of droplets.

On the theoretical side, a recent study (Joanny, 1985) analyzes the motion in a simple inertial regime, at very low temperatures (no normal fluid, and no evaporation), without any vortex nucleation. All the work is restricted to the special case $S = 0$. We shall concentrate here on the *macroscopic regime.*

A force balance argument predicts that the dynamic contact angle *vanishes*. This property is in fact similar to Eq. (4.61) for polymer flow ($d\zeta/dx=0$ at the nominal line position $\mathscr{L}$), and the physical origin is the same: in both cases we have a plug flow and no singularity [in the dissipation, or in the horizontal hydrostatic forces $\zeta(-\partial p/\partial x)$] near the line $\mathscr{L}$. Thus the balance of forces at $\mathscr{L}$ is of the Young type, with no added terms, and $\theta_a=\theta_e=0$.

Let us, then, consider a droplet of original volume $\Omega\cong R_0^3$, spreading to a distance $R(t)\gg R_0$, under the sole action of capillary forces. The initial capillary energy was of order γR_0^2. When this is transformed into kinetic energy, with rms velocity U, we have

$$\Omega\tfrac{1}{2}\rho_L U^2\cong\gamma R_0^2\ , \tag{4.67}$$

$$U\cong\left[\frac{\gamma}{\rho_L R_0}\right]^{1/2}\ . \tag{4.68}$$

The final velocity of the line $\mathscr{L}$ should be constant and given by Eq. (4.68). The detailed shape of the droplet is not simple, but (within the lubrication approximation) Joanny was able to construct exact, self-similar solutions with $\theta_a=0$ and with the velocity (4.68). It would be of interest for the future to investigate the *stability* of these self-similar solutions.

The (more realistic) case where S is *positive* remains completely unexplored. It may be that the energy S is spent in the form of vortex lines nucleated at the solid wall.

F. Unsolved problems

1. Pure fluids

We have seen that a consistent picture may be constructed for the *dry spreading* of a simple fluid on a solid. On the other hand, we noticed that the situation of *moist spreading* requires the specification of a control parameter [H in the notation of Eq. (2.46)] and is thus not unique.

There remains, however, a long list of open questions connected with the spreading of pure fluids, some of which are specified below.

(a) Long-range forces *other than van der Waals* may come into play (especially double-layer effects, if the liquid is water).

(b) All our discussion assumed that the *local dissipation* $T\mathring{\Sigma}_{\rm local}$ near the moving contact line was negligible. This need not be true. Let us list again the different types of dissipation (Sec. IV.C.1):

$$T\mathring{\Sigma}_f=SU\ , \tag{4.69}$$

$$T\mathring{\Sigma}_w=\tfrac{1}{2}\gamma\theta_a^2 U\sim\frac{\eta U^2}{\theta_a}\ , \tag{4.70}$$

$$T\mathring{\Sigma}_{\rm local}=\tfrac{1}{2}\eta_l U^2\ . \tag{4.71}$$

In Eq. (4.71) we tentatively assumed that the local term could be described in terms of a simple friction coefficient η_l (which turns out to have the physical dimensions of a viscosity). If this assumption is correct, we usually expect that, in the limit $\theta_a\to 0$, the hierarchy is

$$T\mathring{\Sigma}_f>T\mathring{\Sigma}_w>T\mathring{\Sigma}_{\rm local} \tag{4.72}$$

provided that

$$\theta_a<\eta/\eta_l\ . \tag{4.73}$$

But this statement may be useless if the local friction cannot be described in the form (4.71), or if the coefficient η_l is much larger than η [so that the conditions (4.73) never hold in practice]. A complete understanding of the local process will probably require calculations of molecular dynamics on specific examples.

(c) *Flow instabilities* may occur, even with viscous fluids. Optical observations by Williams (1977) on spreading droplets of various fluids show a wiggly contact line. This may be interpreted in (at least) three different ways: inhomogeneities in the solid surface (see the discussion on a *static* contact line in Sec. II); solute impurity effects (see Sec. IV.F.2 below); fundamental instabilities in precursor flow: it could be that the films described in Sec. IV.C.3 are intrinsically unstable, even for a pure liquid.

(d) *Transfer via the vapor* may be important even in dry spreading. Although the solid well ahead of the contact line is dry, it may receive a few molecules evaporated from the liquid interface. Even for mildly volatile liquids, this process may renormalize the effective value of the spreading parameter S. Our analysis suggests that this has not much effect on the Tanner law, but that it will change the width d of the precursor film.

(e) All our discussion ignored mechanical losses in the *gas* phase. As early as 1971 Huh and Scriven pointed out that even a gas may become important in the limit of $U>V^*$, where $\theta_a\to\pi$, and where we are actually dealing with a thin film of gas squeezed between liquid and solid. These effects become even more spectacular if we are dealing, not with liquid/gas, but rather with a liquid/liquid system. Pismen and Nir (1982) observed that a simple wedge solution was not acceptable in the macroscopic regime, and that self-similar solutions led to strange "spiral" configurations. Pumir and Pomeau (1984) propose a set of traveling waves following the contact line. This should be checked by experiments on consolute mixtures.

2. Effects of additives in the liquid

a. Volatile impurities

Their role in spreading was noticed early in the optical studies of Bascom *et al.* (1964): certain precursor structures occurred only with impure liquids. The explanation of Bascom *et al.* of these results is based on a local gradient of the surface tension, induced by evaporation near the tip. This interpretation is very plausible. It may be, however, that in some cases the renormalization of S by vapor signals—described in Sec. IV.F.1.c above—plays a role.

b. Surfactants

When they are insoluble in the bulk liquid, surfactants appear only in films at the various interfaces (S/L,S/V,L/V). If we know the surface concentrations Γ_{ij} in these various films, the conservation law gives a condition on the hydrodynamic velocities. Consider, for instance, the very simple case where $\Gamma_{LV} \equiv \Gamma$ is finite, while Γ_{SL} and Γ_{SV} vanish. Then the velocity at the free surface of the liquid must be just equal to the line velocity U, so that the surfactant "never catches up" with the line. This, in turn, imposes a certain modification of the velocity profile in the liquid film and a change of the numerical coefficients in the Tanner law (4.20). Considerations of this type were already present in the work of Huh and Scriven (1971).

For many practical purposes, the effects of surfactants are much more spectacular. For instance Lelah and Marmur (1981) find that a small amount of surfactant (above the critical micelle concentration) gives rise to a hydrodynamic instability in spreading. A well-known class of experiment makes use of a surfactant that attaches slowly to the S/L interface and makes it hydrophobic: a droplet spreads and then retracts. All these effects will require good models of adsorption/desorption kinetics (involving single-surfactant molecules or involving micelles).

c. Polymers

In solution, polymers also can be adsorbed on the S/L interface (and/or on the L/V interface). All the effects mentioned above may appear. Moreover, the hydrodynamic extrapolation length b of Fig. 32 may be drastically reduced by polymer adsorption.

ACKNOWLEDGMENTS

The first version of this review was based on a course given in Paris during 1983—1984, and I wish to thank the participants for their active criticism. Discussions with J. F. Joanny, F. Brochard, and H. Hervet were essential for the construction of a common viewpoint. I have also greatly benefited from written exchanges and/or oral disputes with D. Beaglehole, D. Chan, T. Davis, E. Dussan V., R. Evans, H. Frisch, S. Garoff, B. Hughes, J. Israelashvili, C. Knobler, B. Legait, A. Marmur, B. Maxwell, M. Moldover, M. Nightingale, B. Ninham, Y. Pomeau, F. Rondelez, L. Saraga, M. Schick, L. Schwartz, C. Taupin, G. Teletzke, and B. Widom. A critical reading of the manuscript by M. Adam and by D. Huse has been of considerable help.

REFERENCES

Adamson, A., and A. Zebib, 1980, J. Phys. Chem. **84**, 2619.
Bangham, D., and S. Saweris, 1938, Trans. Faraday Soc. **34**, 554.
Bascom, W., R. Cottington, and C. Singleterry, 1964, in *Contact Angle, Wettability and Adhesion*, edited by F. M. Fowkes, Advances in Chemistry Series, No. 43 (American Chemical Society, Washington, D.C.), p. 355.
Beaglehole, D., 1983, J. Phys. Chem. **87**, 4749.
Benner, R. E., G. F. Teletzke, L. E. Scriven, and H. T. Davis, 1984, J. Chem. Phys. **80**, 589.
Berry, M., 1974, J. Phys. A **7**, 231.
Bouasse, H., 1924, *Capillarité et phénomènes superficiels* (Delagrave, Paris).
Bretherton, F. P., 1961, J. Fluid Mech. **10**, 166.
Brewer, D. F., 1978, in *The Physics of Liquid and Solid Helium*, edited by K. Benneman and J. Ketterson (Wiley, New York), Part II, p. 573.
Brézin, E., B. I. Halperin, and S. Leibler, 1983a, J. Phys. (Paris) **44**, 775.
Brézin, E., B. I. Halperin, and S. Leibler, 1983b, Phys. Rev. Lett. **50**, 1387.
Brochard, F., and P. G. de Gennes, 1984, J. Phys. (Paris) Lett. **45**, L597.
Brockway, L., and R. Jones, 1964, in *Contact Angle, Wettability and Adhesion*, edited by F. M. Fowkes, Advances in Chemistry Series, No. 43 (American Chemical Society, Washington, D.C.), p. 275.
Burton, R. H., M. J. Folkes, K. A. Narh, and A. Keller, 1983, J. Mater. Sci. **18**, 315.
Cahn, J. W., 1977, J. Chem. Phys. **66**, 3667.
Callaghan, I., D. Everett, and J. P. Fletcher, 1983, J. Chem. Soc. Faraday Trans. **79**, 2723.
Callaghan, I. C., and K. W. Baldry, 1978, in *Wetting, Spreading and Adhesion*, edited by J. F. Padday (Academic, New York).
Chang, W. V., Y. M. Chang, L. J. Wang, and Z. G. Wang, 1982, *Organic Coatings and Applied Polymer Science Proceedings* (American Chemical Society, Washington, D.C.), Vol. 47.
Chappuis, J., 1984, in *Multiphase Science and Technology*, edited by G. F. Hewitt, J. Delhaye, and N. Zuber (Hemisphere, New York), p. 387.
Cohn, R., and D. Jacobs, 1983, J. Chem. Phys. **80**, 856.
Cooper, W., and W. Nuttal, 1915, J. Agr. Sci. **7**, 219.
Cox, R. G., 1983, J. Fluid Mech. **131**, 1.
de Gennes, P. G., 1979a, C. R. Acad. Sci. Ser. B **288**, 219.
de Gennes, P. G., 1979b, *Scaling Concepts in Polymer Physics* (Cornell University, Ithaca).
de Gennes, P. G., 1981, J. Phys. (Paris) Lett. **42**, 377.
de Gennes, P. G., 1983, C. R. Acad. Sci. **297 II**, 9.
de Gennes, P. G., 1984a, C. R. Acad. Sci. **298 II**, 111.
de Gennes, P. G., 1984b, C. R. Acad. Sci. **298 II**, 439.
de Gennes, P. G., 1984c, C. R. Acad. Sci. **298 II**, 475.
de Gennes, P. G., 1984d, C. R. Acad. Sci. **300II**, 129.
Deryagin, B., 1940, Zh. Fiz. Khim. **14**, 137.
Deryagin, B., 1955, Kolloidn. Zh. **17**, 191. This review describes the pioneering work of the Russian School.
Deryagin, B., and N. Churaev, 1976, Kolloidn. Zh. **38**, 438.
Deryagin B., Z. Zorin, N. Churaev, and V. Shishin, 1978, in *Wetting, Spreading and Adhesion*, edited by J. F. Padday (Academic, New York).
Dettre, R., and R. Johnson, 1964, in *Contact Angle, Wettability and Adhesion*, edited by F. M. Fowkes, Advances in Chemistry Series, No. 43 (American Chemical Society, Washington, D.C.), p. 136.
Dietrich, S., and M. Schick, 1984, Phys. Rev. B (in press).
Dussan, V. E., 1979, Annu. Rev. Fluid Mech. **11**, 371.
Dussan, V. E., and S. Davis, 1974, J. Fluid Mech. **65**, 71.
Dussan, V. E., and C. Ngan, 1982, J. Fluid Mech. **118**, 27.

Dzyaloshinskii, I. E., E. M. Lifshitz, and L. P. Pitaevskii, 1961, Adv. Phys. **10**, 165.
Ebner, C., and W. F. Saam, 1977, Phys. Rev. Lett. **38**, 1486.
Ebner, C., W. F. Saam, and A. K. Sen, 1984 (to be published).
Evans, R., and U. Marini, 1985, Chem. Phys. Lett. **114**, 415.
Evans, R., and P. Tarazona, 1984, Phys. Rev. Lett. **52**, 557.
Fowkes, F. M., 1962, J. Phys. Chem. **66**, 382.
Fowkes, F. M., 1964, Ed., *Contact Angle, Wettability and Adhesion*, Advances in Chemistry Series, No. 43 (American Chemical Society, Washington, D.C.).
Fox, H., and W. Zisman, 1950, J. Colloid Sci. **5**, 514.
Fritz, G., 1965, Z. Ang. Phys. **19**, 374.
Frumkin, A., 1938, J. Phys. Chem. USSR **12**, 337.
Galt, J., and B. Maxwell, 1964, Mod. Plastics, No. 12.
Garoff, S., and L. Schwartz, 1984, private communication.
Ghiradella, H., W. Radigan, and H. L. Frisch, 1975, J. Colloid Interface Sci. **51**, 522.
Girifalco, L. A., and R. J. Good, 1957, J. Phys. Chem. **61**, 904.
Gittes, F., and M. Schick, 1984, Phys. Rev. B **30**, 209.
Good, R. J., 1964, *Contact Angle, Wettability and Adhesion*, Advances in Chemistry Series, No. 43 (American Chemical Society, Washington, D.C.), p. 74.
Grinstein, G., and S. K. Ma, 1983, Phys. Rev. B **28**, 2588.
Guyon, E., J. Prost, C. Betrencourt, C. Boulet, and B. Volochine, 1982, Eur. J. Phys. **3**, 159.
Hardy, W., 1919, Philos. Mag. **38**, 49.
Hauge, E., and M. Schick, 1983, Phys. Rev. B **27**, 4288.
Heady, R., and J. Cahn, 1972, J. Chem. Phys. **58**, 896.
Hervet, H., and P. G. de Gennes, 1984, C. R. Acad. Sci. **299 II**, 499.
Hocking, L. M., 1976, J. Fluid Mech. **76**, 801.
Hocking, L. M., 1977, J. Fluid Mech. **79**, 209.
Hocking, L. M., 1981, Q. J. Mech. App. Math. **34**, 37.
Hocking, L. M., and A. Rivers, 1982, J. Fluid Mech. **121**, 425.
Hoffman, R., 1975, J. Colloid Interface Sci. **50**, 228.
Huh, C., and S. G. Mason, 1977, J. Colloid Interface Sci. **60**, 11.
Huh, C., and L. E. Scriven, 1971, J. Colloid Interface Sci. **35**, 85.
Huse, D., 1984, private communication.
Hyppia, J., 1948, Anal. Chem. **20**, 1039.
Imry, J., and S. K. Ma, 1975, Phys. Rev. Lett. **35**, 1399.
Israelashvili, J. N., 1982, Adv. Colloid Interface Sci. **16**, 31.
Israelashvili, J. N., 1984, private communication.
Joanny, J. F., 1985, Thèse, Université Paris VI.
Joanny, J. F., and P. G. de Gennes, 1984a, J. Chem. Phys. **81**, 552.
Joanny, J. F., and P. G. de Gennes, 1984b, C. R. Acad. Sci. **299 II**, 279.
Joanny, J. F., and P. G. De Gennes, 1984c, C. R. Acad. Sci. **299II**, 605.
Johnson, R., and R. Dettre, 1964, in *Contact Angle, Wettability and Adhesion*, edited by F. M. Fowkes, Advances in Chemistry Series, No. 43 (American Chemical Society, Washington, D.C.), p. 112.
Kravnik, A. M., and W. R. Schowalter, 1981, J. Rheology **25**, 95.
Kroll, D. M., and T. R. Meister, 1984, Phys. Rev. B (in press).
Landau, L. D., and V. G. Levich, 1942, Acta Physicochim. URSS **17**, 42.
Langmuir, I., 1938, J. Chem. Phys. **6**, 893.
Law, B., 1984 (unpublished).
Legait, B., and P. G. de Gennes, 1984, J. Phys. (Paris) Lett. **45**, 647.
Leibler, S., 1984, Thèse, Orsay.
Lelah, M., and A. Marmur, 1981, J. Colloid Interface Sci. **82**, 518.
Levich, V., 1962, *Physiochemical Hydrodynamics*, 2nd ed. (Prentice Hall, Englewood Cliffs, New Jersey).
Lipowsky, R., and D. M. Kroll, 1984, Phys. Rev. Lett. **52**, 2303.
Lopez, J., C. Miller, and E. Ruckenstein, 1976, J. Colloid Interface Sci. **56**, 460.
Lyklema, J., 1967, in *Study Week on Molecular Forces*, edited by Pontifical Academy of Science (North-Holland, Amsterdam and Wiley-Interscience, New York), pp. 181 and 221.
Marmur, A., 1983, Adv. Colloid Interface Sci. **19**, 75.
Mason, S. G., 1978, in *Wetting, Spreading and Adhesion*, edited by J. F. Padday (Adademic, New York), p. 321.
Michaels, A., and S. Dean, 1962, J. Phys. Chem. **66**, 1790.
Moldover, M., and J. Cahn, 1980, Science **207**, 1073.
Moldover, M., and R. Gammon, 1983, J. Chem. Phys. **80**, 528.
Moldover, M., and J. Schmidt, 1983, J. Chem. Phys. **79**, 379.
Nakanishi, H., and M. Fisher, 1982, Phys. Rev. Lett. **49**, 1565.
Nightingale, M. P., W. F. Saam, and M. Schick, 1983, Phys. Rev. Lett. **51**, 1275.
Ogarev, V., T. Timonina, V. Arslanov, and A. Trapeznikov, 1974, J. Adhesion **6**, 337.
Oliver, J., C. Huh, and S. Mason, 1977, J. Adhesion **8**, 223.
Overbeek, J. T. G., and A. Van Silfhout, 1967, in *Study Week on Molecular Forces*, edited by Pontifical Academy of Sciences (North-Holland, Amsterdam and Wiley-Interscience, New York), p. 143.
Owens, N. F., P. Richmond, and J. Mingins, 1978, in *Wetting, Spreading and Adhesion*, edited by J. F. Padday (Academic, New York), p. 127.
Padday, J. F., 1978, Ed., *Wetting, Spreading and Adhesion* (Academic, New York).
Pandit, R., M. Schick, and M. Wortis, 1982, Phys. Rev. B **26**, 5112.
Pashley, R. M., 1980, J. Colloid Interface Sci. **78**, 246.
Pismen, L. M., and A. Nir, 1982, Phys. Fluids **25**, 3.
Platikhanov, D., M. Nedyalkov, and A. Schelduko, 1980a, J. Colloid Interface Sci. **75**, 612.
Platikhanov, D., M. Nedyalkov, and A. Schelduko, 1980b, J. Colloid Interface Sci. **75**, 620.
Plesner, I., and O. Platz, 1968, J. Chem. Phys. **48**, 5361, footnote II.
Pohl, D., and W. Goldburg, 1982, Phys. Rev. Lett. **48**, 1111.
Pomeau, Y., 1983, C. R. Acad. Sci. **298 II**, 29.
Pomeau, Y., and J. Vannimenus, 1984, J. Colloid Interface Sci. (to be published).
Privman, V., 1984, J. Chem. Phys. **81**, 2463.
Pumir, A., and Y. Pomeau, 1984, C. R. Acad. Sci. (to be published).
Radigan, W., H. Ghiradella, H. L. Frisch, H. Schonhorn, and T. K. Kwei, 1974, J. Colloid Interface Sci. **49**, 241.
Renk, F., P. C. Wayner, Jr., and G. M. Homsy, 1978, J. Colloid Interface Sci. **67**, 408.
Ross, S., and R. Kornbrekke, 1984, J. Colloid Interface Sci. **99**, 446.
Rowlinson, J. S., J. A. Barker, and D. Henderson, 1981, private communication.
Rowlinson, J. S., and B. Widom, 1982, *Molecular Theory of Capillarity* (Oxford University, New York/London).
Ruckenstein, E., and M. Dunn, 1976, J. Colloid Interface Sci. **56**, 460; **59**, 137.
Sawicki, G., 1978, in *Wetting, Spreading and Adhesion*, edited by J. F. Padday (Academic, New York), p. 36.
Schonhorn, H., H. L. Frisch, and T. K. Kwei, 1966, J. Applied

Phys. **37**, 4967.
Snook, I. K., and W. Van Megen, 1979, J. Chem. Phys. **70**, 3099.
Snook, I. K., and W. Van Megen, 1980, J. Chem. Phys. **72**, 2907.
Starov, V. M., 1983, Kolloidnyi J. **45**, 1154.
Sullivan, D. E., 1979, Phys. Rev. B **20**, 3991.
Sullivan, D. E., 1982, Phys. Rev. A **25**, 1669.
Sullivan, D. E., and M. Telo da Gama, 1985, in *Fluctuation Effects on Surfaces*, edited by C. A. Croxston (Wiley, New York).
Tanner, L., 1979, J. Phys. D **12**, 1473.
Tarazona, P., and R. Evans, 1983, Mol. Phys. **48**, 799.
Tarazona, P., M. Telo da Gama, and R. Evans, 1983, Mol. Phys. **49**, 283.
Teletzke, G. F., H. T. Davis, and L. E. Scriven, 1984, J. Colloid Interface Sci. (to be published).
Teletzke, G. F., L. E. Scriven, and H. T. Davis, 1982, J. Chem. Phys. **77**, 5794.
Teletzke, G. F., L. E. Scriven, and H. T. Davis, 1983, J. Chem. Phys. **78**, 1431.
Telo da Gama, M., 1984, Mol. Phys. **52**, 585.
Trillat, J. and R. Fritz, 1937, J. Chim. Phys. **35**, 45.
Tverkrem, J., and D. Jacobs, 1983, Phys. Rev. A **27**, 2773.
Wayner, P. C., 1982, J. Colloid Interface Sci. **88**, 294.
Williams, R., 1977, Nature **266**, 153.
Young, T., 1805, Philos. Trans. R. Soc. London **95**, 65.
Zabel, H., B. Schönfeld, and S. Moss, 1981, J. Phys. Chem. Solids **42**, 897.
Zisman, W., 1964, in *Contact Angle, Wettability and Adhesion*, edited by F. M. Fowkes, Advances in Chemistry Series, No. 43 (American Chemical Society, Washington, D.C.), p. 1.